Exclusive Enteral Nutrition Initiates Protective Microbiome Changes to Induce Remission in Pediatric Crohn's Disease

Häcker, Deborah[1,2]; Siebert, Kolja[3]*; Smith, Byron J[4+]; Köhler, Nikolai[5]; Heimes, Helena[1]; Metwaly, Amira[1]; Mahapatra, Aritra[6]; Hölz, Hannes[3]; De Zen, Federica[3]; Heetmeyer, Jeannine[3]; Socas, Katharina[3]; Le Thi, Giang[3]; Meng, Chen[7]; Kleigrewe, Karin[7]; Pauling, Josch K[5]; Neuhaus, Klaus[6]; List, Markus[8]; Pollard, Katherine S[4,9,10]; Schwerd, Tobias[3&+]; Haller, Dirk[1,2,11&+]*

*&Authors contributed equally, +Corresponding author

[1] Chair of Nutrition and Immunology, TUM School of Life Sciences, Technische Universität München, Freising, Germany
[2] TUMCREATE, 1 CREATE Way, #10-02 CREATE Tower, Singapore 138602
[3] Department of Pediatrics, Dr. von Hauner Children's Hospital, University Hospital, LMU Munich, Germany.
[4] Gladstone Institutes, San Francisco, CA, USA
[5] LipiTUM, Chair of Experimental Bioinformatics, TUM School of Life Sciences, Technical University of Munich, Freising, Germany
[6] Core Facility Microbiome, ZIEL Institute for Food & Health, Technische Universität München, Freising, Germany
[7] Bavarian Center for Biomolecular Mass Spectrometry (BayBioMS), Technische Universität München, Freising, Germany
[8] Data Science in Systems Biology, TUM School of Life Sciences, Technische Universität München, Freising, Germany
[9] University of California, San Francisco, CA, USA
[10] Chan Zuckerberg Biohub
[11] ZIEL Institute for Food & Health, Technische Universität München, Freising, Germany

Abstract

Exclusive enteral nutrition (EEN) is the first-line therapy for pediatric Crohn's disease (CD), but protective mechanisms remain unknown. We established a prospective pediatric cohort (n = 1271 fecal samples) to characterize the function of fecal microbiota and metabolite changes of treatment-naïve CD patients in response to EEN. Integrated multi-omics analysis identified network clusters from individually variable microbiome profiles, with *Lachnospiraceae* and medium chain fatty acids as protective features. Metagenomic analysis identified strain-level dynamics in response to EEN cessation, and 577 gene functions with significant changes in abundance. Functional changes of diet-exposed fecal microbiota were further validated in a combined approach using gut chemostat cultures and microbiota transfer into germ-free *IL-10*-deficient mice. EEN-like and fiber-rich dietary model conditions respectively prevented or induced IBD-like inflammation in gnotobiotic mice. Hence, we provide evidence that EEN therapy operates through explicit functional changes of temporally and individually variable microbiome profiles.

Keywords: Crohn's disease, pediatric, EEN, inflammatory bowel diseases, IBD, diet, fiber, fermentation, gut chemostat, FMT, data integration, microbiome, metabolome, microbial strains

Introduction

Crohn's disease (CD), one of the main entities of inflammatory bowel diseases (IBD), is a chronic and relapsing inflammatory condition of the gastrointestinal tract[1]. Epidemiological studies have demonstrated a significant increase in the incidence of CD in Westernized countries, particularly among the pediatric age group[2,3]. The pathogenesis of IBD involves host genetics and environmental influences, among which diet and the intestinal microbiome are key etiologic factors[4,5].

Exclusive enteral nutrition (EEN) is the first-line treatment for pediatric Crohn's disease (pCD)[6,7], and shows efficacy in adult patients[8]. EEN refers to liquid formulas, which are mostly devoid of fibers[9]. Re-introducing regular diet after 6-8 weeks of EEN often results in recurrence of inflammation and disease activity[10]. EEN has been shown to drive changes in gut microbiota composition[11], but the high relapse rate after cessation of EEN suggests the presence of a CD-conditioned microbiome, which is able to re-establish after dietary intervention[12]. CD is associated with reduced bacterial diversity, compositional and functional changes and the disruption of metabolic circuits between microbiome and host[13–15], however functional evidence for EEN-mediated changes in the microbiome as an underlying cause of therapeutic efficacy is still lacking.

Here, we identify EEN-protective signatures using integrated microbiota and metabolite analysis of treatment-naïve pCD patients. Further, we functionally validate EEN-mediated protective changes in the microbiome using fecal microbiota transfer (FMT) from patients into *ex vivo* gut chemostat and germ-free (GF) *IL10*$^{-/-}$ models. These systems allowed us to investigate the impact of diet on patient-derived fecal microbiota independent of the host, demonstrating that EEN directly shapes individual microbiomes to mediate protective functions in treatment-naïve CD patients.

Results

Microbiota and metabolite profiling identify individual responses to EEN therapy in pCD patients

We established a pediatric IBD cohort and followed 79 IBD patients (37 female, age at study inclusion 12.3 ± 3.8 years, 47 newly diagnosed) longitudinally, classifying them by diagnosis (**Table 1 and Fig. 1A**). Thirty-seven CD patients received EEN, among whom 20 were newly diagnosed and treatment naïve (CD-EEN) (**Table 1** and **Fig. 1A**). Longitudinal fecal samples from this cohort showed no clustering based on disease phenotype (CD, UC/IBDU) or EEN-exposure (16S rRNA gene amplicon sequencing: 804 fecal samples from 78 patients; untargeted metabolomic profiling: 467 fecal samples from 60 patients, **Fig. 1B, C**).

We then focused explicitly on the CD-EEN patients to avoid confounding effects of chronic inflammation and drug exposure. At the end of EEN therapy, disease activity and inflammatory markers improved significantly, resulting in clinical response and induction of remission in 20/20 and 18/20 patients, respectively (**Fig. 1D**). During follow-up, patients received methotrexate (6/20), anti-TNF (13/20), or combination therapies (9/13) as maintenance treatment. Relapse after EEN was observed in 8/20 patients over one-year follow-up (**Fig. 1D**). Two patients switched from Modulen IBD® to Neocate Junior® during EEN due to suspected cow's milk protein allergy.

Analysis of samples before (PreEEN), during (EEN), and after EEN therapy (PostEEN) (microbiota profiling: 291 samples, metabolomic analysis: 145 samples) revealed patient-specific responses (**Fig. 1E, F and J**). Bacterial community richness based on zOTUs at the start of EEN ranged from 82 to 212, and changed individually during formula feeding (**Fig. 1E, Extended Data Fig. 1A**). Reminiscent of the total cohort, dendrograms of microbiota and metabolome analyses showed no EEN-specific clustering (**Fig. 1F, J**). Community richness in samples taken during active CD was lower compared to remission, but not during EEN therapy (**Extended Data Fig. 1B, C**). Despite considerable overlap, multi-dimensional scaling (MDS) plots, microbial profiles were substantially different for: patients with active vs. inactive disease (**Fig. 1G**, n = 281, p = 0.001), during EEN intervention vs. PostEEN (**Fig. 1H,** n = 174**,** p-value = 0.001) and early vs. late during EEN exposure (**Fig. 1I**, n = 70, p-value = 0.017). PCA plots of metabolic profiles (**Fig 1K-M**) showed separation according to disease activity **(Fig 1K**), but weaker partitioning by diet (**Fig 1L**) and no separation by EEN duration (**Fig 1M**).

Integration of microbiota and metabolome data identifies key features of EEN exposure

To identify key features that discriminate EEN and PostEEN, 60 samples were selected from 15 patients at different time points with paired 16S rRNA gene sequencing and untargeted metabolomics data. Network analysis revealed five distinct communities of interlinked features—both zOTUs and metabolites. These integrated sets are hereafter referred to as Community 1 to 5 (**Fig. 2A**). The communities with the highest predictive power based on Receiver Operating Characteristic (ROC)-Area under the Curve (AUC) analysis with the respective feature importance of the integrated data are displayed (**Fig. 2B-G**, Community 4 and 5 are shown in Extended Data Fig. 2A, B). In summary, we identified 16 zOTUs (Community 1: 4 zOTUs; Community 2: 10 zOTUs; Community 4: 1 zOTU; and Community 5: 1 zOTU) relevant for the integrated EEN signature and 9 zOTUs for the integrated PostEEN signature (**Fig. 2H**). The postEEN signature includes zOTUs of the genera *Faecalibacterium, Anaerostipes* and *Bacteroides*. *Blautia* and *Lachnoclostridium* are assigned to EEN and PostEEN. The EEN signature includes four out of the five *Lachnoclostridium* zOTUs, and zOTUs from *Faecalibacterium* sp. UBA1819, *Ruminococcus-torques* group, *Clostridium-*

innocuum group, *Eggerthella*, *Flavonifractor*, *Eisenbergiella*, *Intestinibacter,* and *Thomasclavelia* (**Fig. 2E-G**). Community 1 showed the highest classification power (mean AUC for metabolites of 0.92 ± 0.04 and 0.94 ± 0.05 for zOTUs). Lauric acid and *Faecalibacterium* sp. UBA1819, *Ruminococcus-torques group*, *Eisenbergiella* and *Lachnoclostridium* positively associated with EEN (**Fig. 2E**). In Communities 2 and 3, metabolite features were mostly associated with PostEEN and zOTUs with EEN.

We further addressed patient-specific changes in EEN and PostEEN samples (**Fig. 2H**), emphasizing individual abundance patterns in EEN- or PostEEN-associated taxa. Most metabolites were predictive for PostEEN (n = 68), but we identified 10 metabolites associated to EEN (**Fig. 2E-G**, Extended Data Fig. 2A, B for Community 4 and 5). Palmitoleic acid, lauric acid, decanoic acid, methyl-hexadecanoat and caprylic acid were identified as metabolite features present in Modulen IBD® (**Extended Data Fig. 2C**).

Microbial strains and functions change dramatically at EEN cessation

Next, we collected shotgun metagenomes for 96 CD-EEN patient samples (n=19 patients) and investigated the transition off of EEN at strain-level resolution using StrainFacts[16]. Overall, we observed high strain-level diversity within and between CD-EEN patients. For most species, strains were largely specific to a single patient and appeared in multiple samples from their host, while some samples contained multiple distinct strains (**Supplementary Fig. 2**). Computing the dissimilarity between pairs of samples from the same patient showed that turnover increased with time between samples (**Fig. 3A**). We observed significantly less turnover in samples derived from PostEEN than either during EEN or during the transition off of EEN ($p<10^{-3}$ for both by permutation test). The transition also showed elevated zOTU turnover ($p<10^{-3}$, **Fig. 3B**).

To further connect metagenomic and 16S results, we identified candidate matches where species (based on ubiquitous marker genes) and zOTU relative abundance profiles were highly correlated across samples (**Fig. 3C**). This approach matched 27 zOTUs to one or more metagenomic species (**Fig. 3D; Extended Data Table 1**), accounting for a median of 40% of relative abundance per sample. Thus, metagenomics validated the taxonomic resolution of our microbiome profiling and revealed longitudinal dynamics in microbial communities that was greatest at the transition off of EEN.

To explore these trends, we identified species with extensive strain turnover, large changes in relative abundance at the end of EEN, high mean relative abundance, and high prevalence (**Fig. 3E**, **Extended Data Table 2)**. Many of the top scoring species matched with zOTUs that stood out in network and differential abundance analyses (**Fig. 2**). *Enterocloster bolteae* (formerly *Clostridium bolteae*, belongs to *Lachnoclostridium)* matched with zOTU5 (**Fig. 3C**)

and showed clear shifts in strain composition at or near the transition off of EEN (**Fig. 3F**). In some patients, EEN and PostEEN samples contained similar strains, but the dominant strain changed; in others, a new strain appeared PostEEN that was absent or undetectable during EEN. A second species, *E. clostridioforme* was also matched with zOTU5, but its relative abundance was not significantly affected by EEN cessation. Furthermore, while individual strains of this species did seem to respond to EEN cessation, it had lower strain diversity and turnover overall (**Fig. 3G**). This distinction among strains and between closely related species reinforces the importance of strain-level characterization.

Furthermore, we detected 577 bacterial protein families with substantial changes in abundance (45 increased and 532 decreased) at the transition off of EEN (**Fig. 3H**). Families increased during EEN included COG3845 (mean log2 PostEEN/EEN of -0.68) and COG4603 (-0.65), components of the ABC-type guanosine uptake system. Increases in COG4813 (+1.67), annotated as trehalose utilization protein, and COG3867 (+0.98), arabinogalactan endo-1,4-beta-galactosidase, indicate that microbes encoding these proteins respond to host diet and may play a role in metabolite transformations. These findings are consistent with changes in Guanosine, D-Trehalose, and D-Galacturonic acid found in the metabolite analysis (**Fig. 2A, E**, metabolites 29, 13, and 70, respectively). Altogether, metagenomic analyses demonstrate that gut microbial communities are dynamic at and below the species level and highly influenced by EEN, motivating us to explore their relationship to the clinical efficacy of EEN.

EEN-like diet triggers protective changes in fecal microbiota independent of the host

To further evaluate the impact of EEN on microbiota function, we used continuous culture systems in a gut chemostat model and transferred fecal microbiota into GF WT and *IL10*$^{-/-}$ mice, a microbiota-dependent colitis mouse model, for four weeks (**Fig. 4A**). The *ex vivo* gut chemostat model allowed us to investigate the impact of diet on patient-derived fecal microbiota independent of the host (**Fig. 4B**). Patient sample selection was based on the ability of their stools to replicate disease activity in *IL10*$^{-/-}$ mice after FMT, as previously shown for adult CD patients[17]. First, we chose a fecal sample from a patient with moderate disease activity (model patient 1) based on wPCDAI, fecal calprotectin level and PGA (physician global assessment) prior to EEN therapy (PreEEN), who achieved clinical remission during EEN (**Fig. 4C**). Microbiota transfer of the PreEEN sample induced colonic tissue inflammation in gnotobiotic *IL10*$^{-/-}$ mice (mean histopathology score of 5.3 ± 1.0) but not in WT control mice ($p = 0.002$, mean histopathology score of 1.3 ± 0.5, **Fig. 4C**, H&E **Extended Data Fig. 3A**). *Bacteroides, Lachnoclostridium* and *Blautia* dominated mouse colon content after FMT (**Fig. 4C**). In addition, we selected a stool sample from a patient in clinical remission on EEN who received methotrexate (MTX) as maintenance therapy (model patient 2). Transfer of the fecal

microbiota from this sample failed to induce inflammation in *IL10*$^{-/-}$ and WT mice (**Fig 4D**, H&E **Extended Data Fig. 3A**).

Following transfer into the gut chemostat model, dietary exposure was mimicked using combinations of fiber-free EEN-like and fiber-rich (FR) medium, resembling EEN therapy or the PreEEN/ PostEEN diet, respectively (**Fig. 4B**; right panel). The PreEEN sample from model patient 1 (active disease state, **Fig. 4C**) started on FR (**Fig. 4E**) and revealed decreased bacterial richness of the transferred sample to the vessels during continuous culture with FR medium (**Fig. 4E**, green T), resulting in a community profile similar to that following direct transfer into mice, dominated by *Bacteroides*, *Alistipes* and *Lachnoclostridium* (**Fig. 4E**). This highlights the comparability of the two model systems. After changing to EEN-like medium, the fermenter community showed a proportional increase of *Lachnoclostridium* and decrease of *Alistipes* (**Fig. 4E**). Next, FMT was performed (**Fig. 4E**, marked as T, blue). FR microbiota induced IBD-like tissue pathology in *IL10*$^{-/-}$ mice (mean colon histopathology score = 3.7 ± 1.0, H&E **Extended Data Fig. 3A**), compared to disease-free WT mice (mean colon histopathology score = 1.4 ± 0.5; p = 0.0087, H&E **Extended Data Fig. 3A**). EEN-like medium reversed the inflammatory phenotype of model patient 1 after microbiota transfer from the gut chemostat model to GF *IL10*$^{-/-}$ mice (mean colon histopathology score of *IL10*$^{-/-}$ mice = 2.5 ± 0.8; WT mice = 1.6 ± 0.5, H&E **Extended Data Fig. 3A**, **Fig. 4E**). Thus, *ex vivo* EEN-like intervention recapitulated therapeutic functional changes to the microbiota.

For model patient 2 (EEN induced-remission), the EEN sample was cultured in the gut chemostat on EEN-like medium (**Fig. 4F**). *Ex vivo* fermentation under these conditions for ten days reduced bacterial richness, and remodeling of community structure was observed by changing to FR medium (**Fig. 4F**). FMT of EEN-like microbiota from the gut chemostat model into GF mice did not induce colitis in *IL10*$^{-/-}$ or WT mice (mean colon histopathology score in in *IL10*$^{-/-}$ = 2.0 ± 0.6; WT = 1.0 ± 0.6, H&E **Extended Data Fig. 3B**). In contrast, transfer of FR-conditioned microbiota triggered IBD-like colitis in *IL10*$^{-/-}$, but not in WT mice (mean colon histopathology score in *IL10*$^{-/-}$ = 4.8 ± 1.9 *vs*. WT = 1.5 ± 0.5, p = 0.0152, H&E **Extended Data Fig. 3B**), strongly supporting the hypothesis that diet directly shapes microbiota function. In the following, labeled genera (*) were identified in network data integration associated to the EEN signature. In transfers from both model patients, analyses of differentially abundant bacteria in the mice identified *Lachnoclostridium(*)* as the most dominant and only shared taxon in response to EEN-like medium (**Fig. 4G, H**). Analysis of mice receiving FR-conditioned microbiota showed *Bacteroides* as the most abundant taxon for model patient 1 (**Fig. 4G**) and *Parasutterella* for model patient 2 (**Fi.g 4H**). Both transfer experiments suggest a positive impact of EEN-like diet directly on the fecal microbiota, and indicate fiber reintroduction may trigger relapse.

Relevance of sustained exposure to EEN-like diets to maintain remission after FMT

To address whether sustained EEN exposure improves therapeutic efficacy, we introduced an EEN-like mouse diet one week prior to FMT to evaluate extended dietary effects in WT and *IL10*$^{-/-}$ mice (**Fig. 5A**). Model patient 3 had elevated fecal calprotectin levels of 2828 mg/L at the time of sample collection (**Fig. 5B**, blue arrow) and ongoing mucosal inflammation with macroscopic signs of disease activity (**Fig. 5B**, grey arrow), despite achieving clinical remission under EEN therapy. FMT from model patient 3 induced severe inflammation in recipient *IL10*$^{-/-}$ compared to WT mice (**Fig. 5D**; mean colon histopathology score in *IL10*$^{-/-}$ = 7.3 ± 0.8 *vs*. WT = 1.3 ± 0.5; p = 0.0022, H&E **Extended Data Fig. 3C**), confirming the active disease phenotype. In contrast to model patients 1 and 2 (**Fig. 4**), EEN-like medium did not change the inflammatory phenotype in IBD-susceptible mice after FMT from the chemostat model (chow **Fig. 5E,** mean colon histopathology score in *IL10*$^{-/-}$ = 6.0 ± 1.3 *vs*. WT = 1.6 ± 1.0; p = 0.0006, H&E **Extended Data Fig. 3C**). However, FMT in *IL10*$^{-/-}$ mice fed EEN-like diet significantly lowered disease severity compared to the chow group (EEN-like **Fig. 5E,** mean colon histopathology score in EEN-like-fed *IL10*$^{-/-}$ = 3.2 ± 3.1; p = 0.0407; H&E **Extended Data Fig. 3C**). This suggests that sustained EEN-like feeding suppressed recurrence of disease activity in gnotobiotic mice. Differentially abundant bacteria in both groups confirmed parts of the EEN-signature (**Extended Data Fig. 4A**).

Finally, we selected model patient 4, who achieved remission after EEN, but experienced disease relapse on MTX as maintenance therapy (**Fig. 5C**). Similar to model patient 3, direct FMT induced IBD-like pathology in *IL10*$^{-/-}$ mice (**Fig. 5F,** mean colon histopathology score in *IL10*$^{-/-}$ = 4.3 ± 1.4; p = 0.0087, H&E **Extended Data Fig. 3D**). EEN-like exposure in the gut chemostat model failed to reverse the disease-conditioning nature of the microbiota in chow fed mice, but EEN-like diet significantly reduced the mean colon histopathology score from 6.3 ± 1.5 *IL10*$^{-/-}$ (chow-fed) to 4.3 ± 1.8 (*IL10*$^{-/-}$ EEN-like-fed) (**Fig. 5G**, H&E **Extended Data Fig. 3D**), supporting the hypothesis that EEN-like diets sustain anti-inflammatory activity of the microbiota. Chow and EEN-like fed mice harbored various genera, with *Bacteroides* (chow) and *Parabacteroides* (EEN-like) the most differential abundant taxa (**Extended Data Fig. 4B**).

A combined analyses after FMT identified *Lachnoclostridium(*)* and *Roseburia* as the most abundant taxa in non-inflamed *IL10*$^{-/-}$ mice and *Enterococcus* and *Parasutterella* in inflamed *IL10*$^{-/-}$ mice (**Fig. 5H**). Untargeted metabolomic analyses identified additional differences between inflamed and non-inflamed *IL10*$^{-/-}$ mice (**Fig 5I**). In non-inflamed *IL10*$^{-/-}$ mice, a cluster of deoxycholic acid, cholic acid, chenodeoxycholic acid, lithocholenic acid was observed, and alpha muricholic acid, the most abundant primary bile acid in rodents, and allopurinol clustered in some of the non-inflamed mice. Together, these analyses suggest a functional impact of differences in abundance of taxa and metabolites on the mouse model phenotype.

Discussion

We followed 79 pediatric IBD patients longitudinally, focusing on 20 newly diagnosed CD patients receiving EEN as first-line treatment. Our results corroborate previous observations that EEN is highly effective at inducing remission. We demonstrate that protective functions of EEN therapy are mediated through diet-induced changes in patient microbiomes despite considerable variations in individual microbiota over time. Dietary exposure of patient-derived fecal microbiota in chemostat models and subsequent transfer into IBD-relevant GF mice strongly indicates a causal role of EEN-mediated changes in the microbiome independent of host responses.

Longitudinal sampling revealed an integrated network of taxonomic and metabolomic signatures across pCD patients. In line with previous findings[18], four out of five zOTUs associated with the genus *Lachnoclostridium* were linked to EEN. This may indicate positive effects; low levels of *Lachnoclostridium* have been associated with CD[19]. In addition, this genus was the most abundant in our microbiota transfer experiments, and differentiated non-inflamed from inflamed *IL10*$^{-/-}$ mice, supporting a protective function of *Lachnoclostridium* in EEN therapy. After returning to a regular diet, the microbiomes of CD-EEN patients showed dramatic changes. Taxonomic shifts at the cessation of EEN were highly patient-specific. For example, while in the majority of patients *E. bolteae* (belonging to *Lachnoclostridium* and with zOTU5) was at much higher relative abundance during EEN compared to PostEEN, the dominant strains in many patients changed over this transition, and most strains were detected in just one subject. This diversity and turnover contribute to challenges in predicting taxonomic responses to dietary changes. Antibiotics and pre-existing dysbiosis are both associated with increased strain engraftment in patients receiving fecal microbiota transplants[20]. Likewise, the microbiome perturbation caused by EEN—and its cessation—may encourage strain turnover, with potentially complex consequences for microbial function after therapy.

Beyond taxonomic alterations, we identified 10 metabolites associated with EEN treatment and 68 metabolites associated with PostEEN samples. Independently, metagenomic analysis highlighted 577 bacterial gene functions with substantial changes in response to EEN, suggesting specific metabolic adaptations of the microbiota to host diets. Modulen IBD® is characterized by easily digestible carbohydrates and high fat content, including medium-chain triglycerides[9]. Our integrated network analysis highlighted caprylic (CA, C8:0), decanoic (DA C10:0), and lauric (LA, C12:0) acids as associated with protective EEN signatures. These medium-chain fatty acids (MCFAs) are also part of the EEN formula. MCFAs, in particular those mentioned, show taxon-specific anti-bacterial and anti-inflammatory effects, such as growth inhibition of *Clostridioides difficile* and other Gram-positive bacteria. MCFAs damage bacterial cell membranes/walls and inhibit host pro-inflammatory cytokines and transcription factors like

NF-κB[21–23]. Diets high in fat trigger release of bile acids[24], providing a rationale for *Clostridium innocuum* and *Hungatella hathewayi* to be part of protective EEN signatures[25,26]. Concordantly, our untargeted metabolomics analysis identified three primary and two secondary bile acids in non-inflamed *IL10*$^{-/-}$ mice. Secondary bile acids are thought to promote wound healing and epithelial regeneration[24]. In a recent study (FARMM), EEN specifically affected amino acid pathways in the microbiome creating a metabolite milieu low in bacteria-derived indoles[27]. In addition, EEN-related protective effects in *IL10*$^{-/-}$ mice are partially mediated by isobutyrate production[28], supporting the hypothesis that microbiota and metabolite changes contribute to the EEN therapeutic efficacy.

In healthy humans, dietary fiber intake supports beneficial functions of the gastrointestinal tract[29]. In animal models, low fiber diets induce adverse microbiota changes associated with impaired intestinal barrier integrity and bacteria-related mucus degradation[30,31], highlighting the fiber paradox in understanding EEN-mediated anti-inflammatory mechanisms in IBD. Dietary fiber consists of complex carbohydrates which are resistant to digestion and absorption by the host. However, dietary fiber degradation and availability for the host depends on the fermenting potential of host-specific microbial communities, which are modified by intestinal inflammation[29,32,33]. Using the combined gut chemostat-to-mouse transfer approach, we showed that a fiber-free EEN-like medium maintains the anti-inflammatory and remitting phenotype associated with EEN therapy. Concordantly, the protective effect of EEN-conditioned microbiota is reversible upon exposure to fiber-rich diet. Recent studies have demonstrated that fiber-free diets prevent and diminish the colonization of identified pathobionts in different CD-like mouse models[34,35], supporting our hypothesis that EEN therapy directly creates protective niches in the gut microbiome. Preserving beneficial microbiome signatures after cessation of EEN may be a new approach to guide mucosal healing and remission in pCD[36]. In our IBD cohort, 40% (8/20) of pCD patients relapsed within the first year after EEN treatment, highlighting the necessity to maintain remitting conditions. Our data support the development of tailored maintenance strategies in pCD involving combinations of personalized nutritional and bacterial interventions.

Funding

Funded by the Deutsche Forschungsgemeinschaft (DFG, German Research Foundation) – project number 395357507 (SFB 1371, Microbiome Signatures) and the Leona M. and Harry B. Helmsley Charitable Trust (project numbers 2847 and 2304-05970). TS is supported by the Medical & Clinician Scientist Program (MCSP) of the Faculty of Medicine at LMU Munich.

Conflict of interest

DHaller served on the Microbiome Expert Panel from Reckitt Benckiser Health Limited. TS received lecture honoraria from Nutricia and MSD and travel support from Abbvie and Ferring outside the submitted work.

Acknowledgement

We thank the patients and their families for participating in our research.

Author contribution

DHaecker, KSiebert, TS and DHaller wrote the manuscript, designed the study and experiments; KSiebert, HHölz, JHeetmeyer, FDeZen, GLeThi, TS: collected and prepared clinical data and samples, accompanied, followed and characterized patients, analysis of clinical data; HHölz, TS recruited patients; DHaecker, HHeimes, AMetwaly and DHaller performed and interpreted mouse and fermenter experiments; DHaecker performed 16S rRNA gene amplicon and corresponding statistical analysis; CM, KSocas, KK performed metabolomics with statistical analysis; KSiebert, DHaecker, NK, AMetwly, ML responsible for integration of clinical metadata with 16S and metabolomics as well as sample selection and performance of data integration and network analysis; NK, ML, PJK performed 16S & untargeted metabolomics data integration, untargeted metabolomics data analyses; BS, AMahapatra, KSP performed metagenomic sequencing and analyses; KN provided 16S rRNA gene amplicon and metagenome sequencing and support for analysis; DHaecker, KSiebert, BS, NK, KSP, TS and DHaller evaluated and interpreted data; All authors provided input on the manuscript, critically revised and approved the final version of the manuscript.

ORCID IDs

Deborah Häcker https://orcid.org/0000-0001-7914-9470
Kolja Siebert https://orcid.org/0009-0005-8083-7074
Byron J Smith https://orcid.org/0000-0002-0182-404X
Nikolai Köhler https://orcid.org/0000-0002-5103-883X
Amira Metwaly https://orcid.org/0000-0001-5740-0230
Hannes Hoelz https://orcid.org/0000-0002-7208-6195
Jeannine Heetmeyer https://orcid.org/0000-0002-0599-9613
Katharina Socas https://orcid.org/0009-0003-8625-4879
Giang Le Thi https://orcid.org/0000-0002-2504-9551

Chen Meng https://orcid.org/0000-0002-5968-6719
Karin Kleigrewe https://orcid.org/0000-0002-7718-0252
Klaus Neuhaus https://orcid.org/0000-0002-6020-2814
Markus List https://orcid.org/0000-0002-0941-4168
Katherine S Pollard https://orcid.org/0000-0002-9870-6196
Tobias Schwerd https://orcid.org/0000-0002-2281-4852
Dirk Haller http://orcid.org/0000-0002-6977-4085

References

1. Torres, J., Mehandru, S., Colombel, J. F. & Peyrin-Biroulet, L. Crohn's disease. *Lancet* **389**, 1741–1755 (2017).

2. Kuenzig, M. E. *et al.* Twenty-first Century Trends in the Global Epidemiology of Pediatric-Onset Inflammatory Bowel Disease: Systematic Review. *Gastroenterology* **162**, 1147-1159.e4 (2022).

3. Kaplan, G. G. & Ng, S. C. Understanding and Preventing the Global Increase of Inflammatory Bowel Disease. *Gastroenterology* **152**, 313-321.e2 (2017).

4. Liu, Z. *et al.* Genetic architecture of the inflammatory bowel diseases across East Asian and European ancestries. *Nat Genet* **55**, 796 (2023).

5. Renz, H. *et al.* Gene-environment interactions in chronic inflammatory disease. *Nature Immunology 2011 12:4* **12**, 273–277 (2011).

6. Van Rheenen, P. F. *et al.* The Medical Management of Paediatric Crohn's Disease: an ECCO-ESPGHAN Guideline Update. *J Crohns Colitis* **15**, 171–194 (2020).

7. Agrawal, M., Spencer, E. A., Colombel, J. F. & Ungaro, R. C. Approach to the Management of Recently Diagnosed Inflammatory Bowel Disease Patients: A User's Guide for Adult and Pediatric Gastroenterologists. *Gastroenterology* **161**, 47–65 (2021).

8. Bischoff, S. C. *et al.* ESPEN guideline on Clinical Nutrition in inflammatory bowel disease. *Clin Nutr* **42**, 352–379 (2023).

9. Logan, M. *et al.* Analysis of 61 exclusive enteral nutrition formulas used in the management of active Crohn's disease—new insights into dietary disease triggers. *Aliment Pharmacol Ther* **51**, 935–947 (2020).

10. Logan, M. *et al.* The reduction of faecal calprotectin during exclusive enteral nutrition is lost rapidly after food re-introduction. *Aliment Pharmacol Ther* **50**, 664 (2019).

11. Schwerd, T. *et al.* Exclusive enteral nutrition in active pediatric Crohn disease: Effects on intestinal microbiota and immune regulation. *Journal of Allergy and Clinical Immunology* **138**, 592–596 (2016).

12. Frivolt, K. *et al.* Repeated exclusive enteral nutrition in the treatment of paediatric Crohn's disease: Predictors of efficacy and outcome. *Aliment Pharmacol Ther* **39**, 1398–1407 (2014).

13. Metwaly, A., Reitmeier, S. & Haller, D. Microbiome risk profiles as biomarkers for inflammatory and metabolic disorders. *Nature Reviews Gastroenterology & Hepatology 2022 19:6* **19**, 383–397 (2022).

14. Schirmer, M., Garner, A., Vlamakis, H. & Xavier, R. J. Microbial genes and pathways in inflammatory bowel disease. *Nat Rev Microbiol* **17**, 497 (2019).

15. Lavelle, A. & Sokol, H. Gut microbiota-derived metabolites as key actors in inflammatory bowel disease. *Nature Reviews Gastroenterology & Hepatology 2020 17:4* **17**, 223–237 (2020).

16. Smith, B. J., Li, X., Shi, Z. J., Abate, A. & Pollard, K. S. Scalable Microbial Strain Inference in Metagenomic Data Using StrainFacts. *Frontiers in Bioinformatics* **2**, (2022).

17. Metwaly, A. *et al.* Integrated microbiota and metabolite profiles link Crohn's disease to sulfur metabolism. *Nature Communications 2020 11:1* **11**, 1–15 (2020).

18. Jiang, J., Chen, L., Chen, Y. & Chen, H. Exclusive enteral nutrition remodels the intestinal flora in patients with active Crohn's disease. *BMC Gastroenterol* **22**, (2022).

19. Vich Vila, A. *et al.* Gut microbiota composition and functional changes in inflammatory bowel disease and irritable bowel syndrome. *Sci Transl Med* **10**, (2018).

20. Podlesny, D. *et al.* Identification of clinical and ecological determinants of strain engraftment after fecal microbiota transplantation using metagenomics. *Cell Rep Med* **3**, 100711 (2022).

21. Yang, H. T. *et al.* Lauric acid is an inhibitor of Clostridium difficile growth in vitro and reduces inflammation in a mouse infection model. *Front Microbiol* **8**, 2635 (2018).

22. Kabara, J. J., Swieczkowski, D. M., Conley, A. J. & Truant, J. P. Fatty acids and derivatives as antimicrobial agents. *Antimicrob Agents Chemother* **2**, 23–28 (1972).

23. Huang, W. C. *et al.* Anti-bacterial and anti-inflammatory properties of capric acid against Propionibacterium acnes: A comparative study with lauric acid. *J Dermatol Sci* **73**, 232–240 (2014).

24. Sorrentino, G. *et al.* Bile Acids Signal via TGR5 to Activate Intestinal Stem Cells and Epithelial Regeneration. *Gastroenterology* **159**, 956-968.e8 (2020).

25. Xiao, F. *et al.* Exclusive Enteral Nutrition Exerts Anti-Inflammatory Effects through Modulating Microbiota, Bile Acid Metabolism, and Immune Activities. *Nutrients* **14**, 4463 (2022).

26. Lv, Y. *et al.* The impact of exclusive enteral nutrition on the gut microbiome and bile acid metabolism in pediatric Crohn's disease. *Clinical Nutrition* **42**, 116–128 (2023).

27. Tanes, C. *et al.* Role of dietary fiber in the recovery of the human gut microbiome and its metabolome. *Cell Host Microbe* **29**, 394-407.e5 (2021).

28. Pereira, G. V. *et al.* Unravelling specific diet and gut microbial contributions to inflammatory bowel disease. *bioRxiv* 2022.04.03.486886 (2022) doi:10.1101/2022.04.03.486886.

29. Gill, S. K., Rossi, M., Bajka, B. & Whelan, K. Dietary fibre in gastrointestinal health and disease. *Nature Reviews Gastroenterology & Hepatology 2020 18:2* **18**, 101–116 (2020).

30. Schroeder, B. O. *et al.* Bifidobacteria or Fiber Protects against Diet-Induced Microbiota-Mediated Colonic Mucus Deterioration. *Cell Host Microbe* **23**, 27-40.e7 (2018).

31. Desai, M. S. *et al.* A Dietary Fiber-Deprived Gut Microbiota Degrades the Colonic Mucus Barrier and Enhances Pathogen Susceptibility. *Cell* **167**, 1339-1353.e21 (2016).

32. Haskey, N., Gold, S. L., Faith, J. J. & Raman, M. To Fiber or Not to Fiber: The Swinging Pendulum of Fiber Supplementation in Patients with Inflammatory Bowel Disease. *Nutrients 2023, Vol. 15, Page 1080* **15**, 1080 (2023).

33. Armstrong, H., Mander, I., Zhang, Z., Armstrong, D. & Wine, E. Not All Fibers Are Born Equal; Variable Response to Dietary Fiber Subtypes in IBD. *Front Pediatr* **8**, 620189 (2021).

34. Kuffa, P. *et al.* Fiber-deficient diet inhibits colitis through the regulation of the niche and metabolism of a gut pathobiont. *Cell Host Microbe* (2023) doi:10.1016/J.CHOM.2023.10.016.

35. Metwaly, A. *et al.* Diet prevents the expansion of segmented filamentous bacteria and ileo-colonic inflammation in a model of Crohn's disease. *Microbiome* **11**, 66 (2023).

36. Turner, D. *et al.* STRIDE-II: An Update on the Selecting Therapeutic Targets in Inflammatory Bowel Disease (STRIDE) Initiative of the International Organization for the Study of IBD (IOIBD): Determining Therapeutic Goals for Treat-to-Target strategies in IBD. *Gastroenterology* **160**, 1570–1583 (2021).

458 **Methods References**

459 37. Levine, A. *et al.* ESPGHAN Revised Porto Criteria for the Diagnosis of Inflammatory
460 Bowel Disease in Children and Adolescents. *J Pediatr Gastroenterol Nutr* **58**, 795–806
461 (2014).

462 38. Turner, D. *et al.* Management of paediatric ulcerative colitis, part 1: Ambulatory Care-An
463 Evidence-based Guideline From European Crohn's and Colitis Organization and
464 European Society of Paediatric Gastroenterology, Hepatology and Nutrition. *J Pediatr*
465 *Gastroenterol Nutr* **67**, 257–291 (2018).

466 39. Turner, D. *et al.* Management of paediatric ulcerative colitis, part 2: Acute severe colitis
467 - An evidence-based consensus guideline from the european Crohn's and colitis
468 organization and the european society of paediatric gastroenterology, hepatology and
469 nutrition. *J Pediatr Gastroenterol Nutr* **67**, 292–310 (2018).

470 40. Schult, D. *et al.* Gut bacterial dysbiosis and instability is associated with the onset of
471 complications and mortality in COVID-19. *Gut Microbes* **14**, (2022).

472 41. Püngel, D. *et al.* Bifidobacterium breve UCC2003 Exopolysaccharide Modulates the
473 Early Life Microbiota by Acting as a Potential Dietary Substrate. *Nutrients* **12**, 948
474 (2020).

475 42. Macfarlane, G. T., Macfarlane, S. & Gibson, G. R. Validation of a three-stage compound
476 continuous culture system for investigating the effect of retention time on the ecology
477 and metabolism of bacteria in the human colon. *Microb Ecol* **35**, 180–187 (1998).

478 43. Gibson, G. R. & Wang, X. Enrichment of bifidobacteria from human gut contents by
479 oligofructose using continuous culture. *FEMS Microbiol Lett* **118**, 121–127 (1994).

480 44. Cinquin, C., Le Blay, G., Fliss, I. & Lacroix, C. Immobilization of infant fecal microbiota
481 and utilization in an in vitro colonic fermentation model. *Microb Ecol* **48**, 128–138 (2004).

482 45. Poeker, S. A. *et al.* Stepwise Development of an in vitro Continuous Fermentation Model
483 for the Murine Caecal Microbiota. *Front Microbiol* **10**, (2019).

484 46. Reitmeier, S., Kiessling, S., Neuhaus, K. & Haller, D. Comparing Circadian Rhythmicity
485 in the Human Gut Microbiome. *STAR Protoc* **1**, 100148 (2020).

486 47. Lagkouvardos, I., Fischer, S., Kumar, N. & Clavel, T. Rhea: A transparent and modular
487 R pipeline for microbial profiling based on 16S rRNA gene amplicons. *PeerJ* **2017**,
488 (2017).

489 48. Chen, J. *et al.* Associating microbiome composition with environmental covariates using
490 generalized UniFrac distances. *Bioinformatics* **28**, 2106–2113 (2012).

491 49. Jost, L. Partitioning diversity into independent alpha and beta components. *Ecology* **88**,
492 2427–2439 (2007).

493 50. Subramanian, B., Gao, S., Lercher, M. J., Hu, S. & Chen, W. H. Evolview v3: a
494 webserver for visualization, annotation, and management of phylogenetic trees. *Nucleic*
495 *Acids Res* **47**, W270–W275 (2019).

496 51. Segata, N. *et al.* Metagenomic biomarker discovery and explanation. *Genome Biol* **12**,
497 R60 (2011).

498 52. Bolger, A. M., Lohse, M. & Usadel, B. Trimmomatic: a flexible trimmer for Illumina
499 sequence data. *Bioinformatics* **30**, 2114–2120 (2014).

500 53. Langmead, B. & Salzberg, S. L. Fast gapped-read alignment with Bowtie 2. *Nature*
501 *Methods 2012 9:4* **9**, 357–359 (2012).

502 54. Shi, Z. J., Dimitrov, B., Zhao, C., Nayfach, S. & Pollard, K. S. Fast and accurate
503 metagenotyping of the human gut microbiome with GT-Pro. *Nature Biotechnology 2021*
504 *40:4* **40**, 507–516 (2021).

505 55. Almeida, A. *et al.* A unified catalog of 204,938 reference genomes from the human gut
506 microbiome. *Nature Biotechnology 2020 39:1* **39**, 105–114 (2020).

507 56. Zhao, C., Dimitrov, B., Goldman, M., Nayfach, S. & Pollard, K. S. MIDAS2: Metagenomic
508 Intra-species Diversity Analysis System. *Bioinformatics* **39**, (2023).

509 57. Reiter, S. *et al.* Development of a Highly Sensitive Ultra-High-Performance Liquid
510 Chromatography Coupled to Electrospray Ionization Tandem Mass Spectrometry
511 Quantitation Method for Fecal Bile Acids and Application on Crohn's Disease Studies. *J*
512 *Agric Food Chem* **69**, 5238–5251 (2021).

513 58. Weiss, A. S. *et al.* In vitro interaction network of a synthetic gut bacterial community. *The*
514 *ISME Journal 2021 16:4* **16**, 1095–1109 (2021).

515 59. Singh, A. *et al.* DIABLO: an integrative approach for identifying key molecular drivers
516 from multi-omics assays. *Bioinformatics* **35**, 3055–3062 (2019).

517 60. Benjamini, Y. & Hochberg, Y. Controlling the False Discovery Rate: A Practical and
518 Powerful Approach to Multiple Testing. *Journal of the Royal Statistical Society: Series B*
519 *(Methodological)* **57**, 289–300 (1995).

61. Blondel, V. D., Guillaume, J. L., Lambiotte, R. & Lefebvre, E. Fast unfolding of communities in large networks. *Journal of Statistical Mechanics: Theory and Experiment* **2008**, P10008 (2008).

62. Csárdi, G. & Nepusz, T. The igraph software package for complex network research. *InterJournal, Complex Systems* **5**, 1–9 (2006).

63. Hagberg, A. A., Lanlgov -Los, Schult, D. A. & Swart, P. J. S. Exploring Network Structure, Dynamics, and Function using NetworkX. (2008).

64. Yoon, S. H. *et al.* Introducing EzBioCloud: A taxonomically united database of 16S rRNA gene sequences and whole-genome assemblies. *Int J Syst Evol Microbiol* **67**, 1613–1617 (2017).

		CD (N=45)	CD-EEN (N=20)		UC /IBDU (N=34, 29/5)
Sex	Male	24 (53%)	11 (55%)		18 (53%)
	Female	21 (47%)	9 (45%)		16 (47%)
Age at diagnosis (years)		11.9 (3.5)	12.4 (3.2)		9.8 (4.4)
Age at study inclusion (years)		13.3 (3.3)	12.5 (3.1)		11.0 (4.3)
First degree family history of IBD		8 (18%)	3 (15%)		7 (21%)
Mean height (Z Score)		-0.06 (1.05)	0.17 (1.06)		0.22 (1.11)
Mean weight (Z score)		-0.51 (1.29)	-0.57 (1.32)		-0.24 (1.07)
Mean body-mass index (Z score)		-0.75 (1.49)	-0.95 (1.44)		-0.56 (1.02)
Disease characteristics					
Location - lower GI [1]	None	1 (2%)	1 (5%)	Proctitis	0
	Ileum only	8 (18%)	3 (15%)	Left sided	4 (12%)
	Colon only	8 (18%)	5 (25%)	Extensive	7 (21%)
	Ileocolonic	28 (62%)	11 (55%)	Pancolitis	23 (67%)
Location - upper GI [1]	Proximal (n, %)	34 (76%)	18 (90%)		
	Distal (n, %)	11 (24%)	6 (30%)		
Behavior [1]	Nonstricturing-nonpenetrating	37 (82%)	17 (85%)	Never severe	24 (71%)
	Stricturing	5 (11%)	2 (10%)	Ever severe	10 (29%)
	Penetrating	1 (2%)	1 (5%)		
	Stricturing and penetrating	2 (4%)	0		
Perianal involvement		9 (20%)	4 (20%)		
Evidence of growth delay		11 (24%)	4 (20%)		
Extraintestinal manifestations [2]		8 (18%)	5 (25%)		5 (15%)
Previous surgery		5 (11%)	0		0
Disease activity					
Median wPCDAI		40 (30 to 52.5)	43.8 (38.1 to 51.3)	PUCAI	42.5 (25 to 56.3)
Inactive (wPCDAI <12.5)		3 (7%)	0 (%)	Inactive (PUCAI <10)	3 (9%)
Mild (wPCDAI 12.5 to 40)		23 (51%)	8 (40%)	Mild (PUCAI 10 to 34)	11 (32%)
Moderate (wPCDAI 42.5 to 57.5)		11 (24%)	8 (40%)	Moderate (PUCAI 35 to 64)	13 (38%)
Severe (wPCDAI >57.5)		8 (18%)	4 (20%)	Severe (PUCAI ≥65)	7 (21%)
Baseline laboratory data					
Mean CRP (mg/dl)		2.7 (3.5)	3.7 (4.3)		1.4 (2.6)
Mean ESR (mm/h)		31.4 (21.6)	36.8 (21.3)		29.9 (27.7)
Elevated inflammatory marker [3]		31 (69%)	18 (90%)		20 (59%)
Mean albumin (g/dL)		4.1 (0.7)	4.1 (0.5)		4.3 (0.6)
Hypoalbuminaemia (<3.5 g/dL)		6 (13%)	2 (10%)		2 (6%)
Mean hemoglobin, g/dL		11.9 (1.8)	11.7 (1.6)		11.2 (2.7)
Anemia (<10 g/dL)		6 (13%)	3 (15%)		9 (26%)
Median fecal calprotectin (IQR)		954 (166 to 3041)	2068 (825 to 7362)		1133 (430 to 2914)
Treatment					
Newly diagnosed		30 (67%)	20 (100%)		17 (50%)
EEN therapy duration in days			52 (19)		n.a.
Previous therapies	EEN	11 (%)	-		n.a.
	5-ASA	2 (4%)	-		4 (12%)
	Steroids	8 (18%)	-		9 (26%)

	IM	7 (16%)	-		1 (3%)
	Previous biologics	3 (7%)	-		1 (3%)
Ongoing therapies at time of study recruitment	5-ASA	4 (9%)	-		13 (38%)
	Steroids	1 (2%)	-		4 (12%)
	IM	4 (9%)	-		3 (9%)
	Anti-TNF	5 (11%)	-		3 (9%)

Table 1: Patient characterization:

Data are N (%), mean (SD), or median (IQR 25th to 75th percentile). 5-ASA, 5-aminosalicylic acids; BMI, body-mass index; CRP, C-reactive protein; EEN, exclusive enteral nutrition; ESR, erythrocyte sedimentation rate; IBD, inflammatory bowel disease; IM, immunomodulater (e.g., azathioprine, methotrexate); PUCAI, Pediatric Ulcerative Colitis Activity Index; TNF, tumor necrosis factor; wPCDAI, weighted Pediatric Crohn's Disease Activity Index. [1] As per Paris classification. [2] Five patients had joint manifestations, two had eye manifestations, eight had skin manifestations, one had autoimmune sclerosing cholangitis and one had autoimmune hepatitis. [3] CRP ≥ 0.5 mg/L or ESR ≥ 25 mm/h.

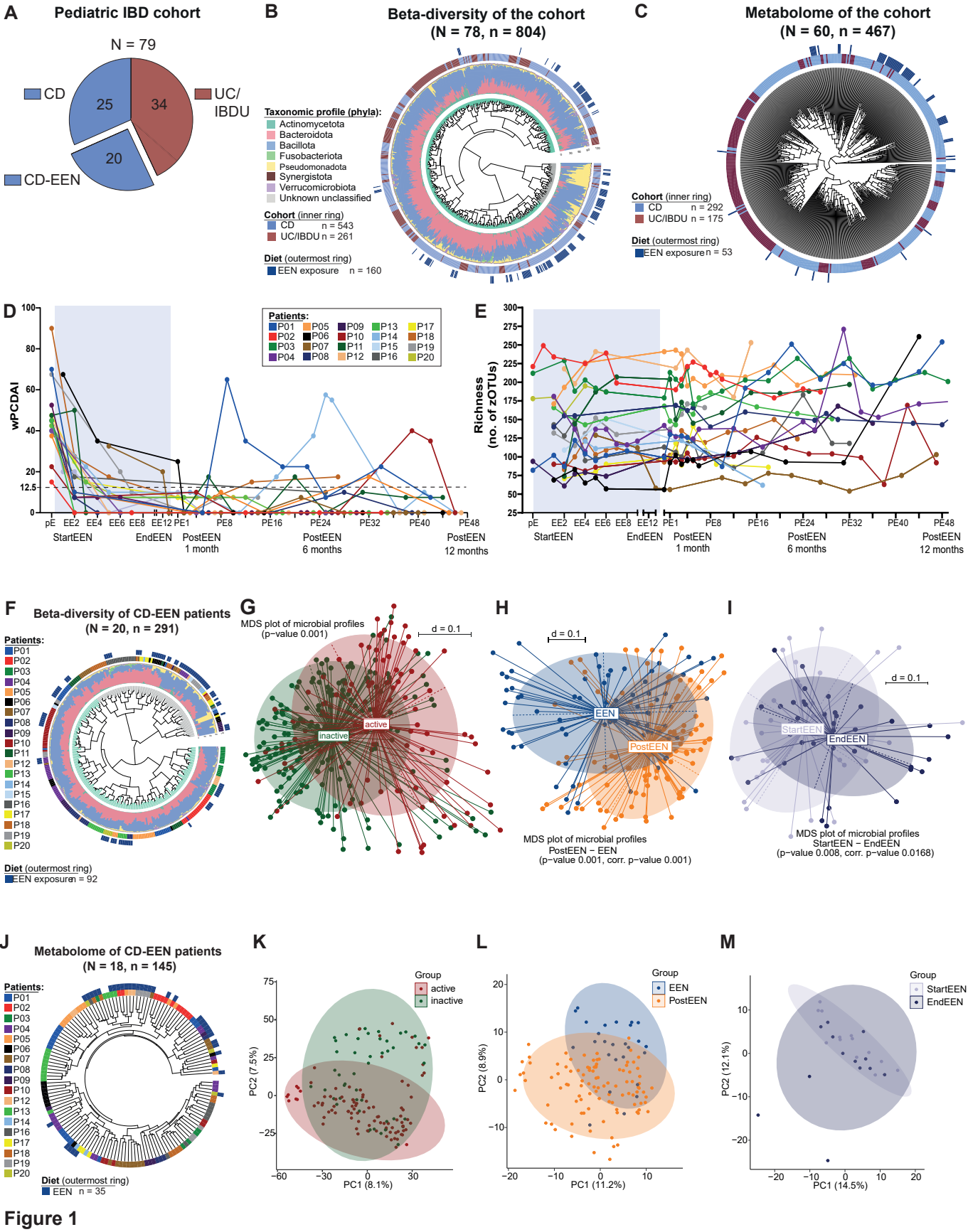
A
Pediatric IBD cohort
N = 79
CD
25
34
UC/
IBDU
20
CD-EEN
B
Beta-diversity of the cohort
(N = 78, n = 804)
Taxonomic profile (phyla):
Actinomycetota
Bacteroidota
Bacillota
Fusobacteriota
Pseudomonadota
Synergistota
Verrucomicrobiota
Unknown unclassified
Cohort (inner ring)
CD n = 543
UC/IBDU n = 261
Diet (outermost ring)
EEN exposure n = 160
C
Metabolome of the cohort
(N = 60, n = 467)
Cohort (inner ring)
CD n = 292
UC/IBDU n = 175
Diet (outermost ring)
EEN exposure n = 53
D
wPCDAI
Patients:
P01 P02 P03 P04 P05 P06 P07 P08 P09 P10 P11 P12 P13 P14 P15 P16 P17 P18 P19 P20
pE EE2 EE4 EE6 EE8 EE12 PE1 PE8 PE16 PE24 PE32 PE40 PE48
StartEEN
EndEEN
PostEEN 1 month
PostEEN 6 months
PostEEN 12 months
E
Richness (no. of zOTUs)
pE EE2 EE4 EE6 EE8 EE12 PE1 PE8 PE16 PE24 PE32 PE40 PE48
StartEEN
EndEEN
PostEEN 1 month
PostEEN 6 months
PostEEN 12 months
F
Beta-diversity of CD-EEN patients
(N = 20, n = 291)
Patients:
P01 P02 P03 P04 P05 P06 P07 P08 P09 P10 P11 P12 P13 P14 P15 P16 P17 P18 P19 P20
Diet (outermost ring)
EEN exposure n = 92
G
MDS plot of microbial profiles
(p−value 0.001)
d = 0.1
active
inactive
H
d = 0.1
EEN
PostEEN
MDS plot of microbial profiles
PostEEN − EEN
(p−value 0.001, corr. p−value 0.001)
I
d = 0.1
StartEEN
EndEEN
MDS plot of microbial profiles
StartEEN − EndEEN
(p−value 0.008, corr. p−value 0.0168)
J
Metabolome of CD-EEN patients
(N = 18, n = 145)
Patients:
P01 P02 P03 P04 P05 P06 P07 P08 P09 P10 P12 P13 P14 P16 P17 P18 P19 P20
Diet (outermost ring)
EEN n = 35
K
Group
active
inactive
PC2 (7.5%)
PC1 (8.1%)
L
Group
EEN
PostEEN
PC2 (8.9%)
PC1 (11.2%)
M
Group
StartEEN
EndEEN
PC2 (12.1%)
PC1 (14.5%)

Figure 1

Fig. 1: Fecal microbial and metabolic changes in response to EEN.

A *Patients of the Pediatric IBD cohort.* ***B*** *Beta-diversity analysis of the fecal microbiota in IBD patients. The circular dendrogram shows differences in beta-diversity from the longitudinal microbial profiling based on generalized UniFrac distances between 804 samples of 78 patients of the cohort. Taxonomic composition of fecal samples at the phylum level is shown as color-coded stacked bar blots around the dendrogram. Bars in the first outer ring of the figure show disease phenotypes (CD, UC/IBDU) and EEN treatment in the second outer ring.* ***C*** *Complete clustering of untargeted metabolomic samples with Euclidean distance for 467 longitudinal fecal samples from 60 IBD patients, visualized in a circular tree.* ***D – I*** *Visualizations of beta-diversities concerning samples from the 20 newly diagnosed pCD patients receiving EEN therapy.* ***D*** *Weighted pediatric Crohn's Disease activity index (wPCDAI) over time (EEN shaded blue), remission achieved below 12.5 points (dashed line). pE = PreEEN, EE = EEN, PE = PostEEN.* ***E*** *Alpha-diversity plotted as richness (number of zOTUs) over time as in D.* ***F*** *Beta-diversity analysis of the fecal microbiota samples. The circular dendrogram shows differences in beta-diversities from the longitudinal microbial profiling based on generalized UniFrac distances between the 291 stool samples of the 20 patients. Indicated in color code are the patients and samples collected during EEN. Color code of taxonomic composition at phylum level as in B.* ***G – I*** *Beta-diversity MDS plots:* ***G*** *Active versus inactive samples (n = 281),* ***H*** *Samples during EEN (at least two weeks on EEN, n = 73) versus PostEEN (two weeks after end of EEN-induced remission, n = 101),* ***I*** *Start of EEN (StartEEN, n = 34) versus the very last matching samples under EEN (week 6-9, depending on the individual therapy of patients; EndEEN, n = 36).* ***J – M:*** *Visualization of untargeted metabolome samples from 18 newly diagnosed pediatric CD patients receiving EEN therapy:* ***J*** *Complete clustering with Euclidean distance of longitudinal samples from 18 CD-EEN patients (n = 145),* ***K – M*** *Analyses of untargeted metabolomics with representative PCA plots comparing different groups (color codes as indicated). Axes indicate principal components (PC), with PC1 representing the most variation (%) and PC2 representing the second most variation (%).* ***K*** *Samples during active (n = 99) vs. inactive (n = 46) disease.* ***L*** *Samples during EEN (n = 26) and PostEEN (n = 100; same cut off as in H),* ***M*** *Start (n = 13) vs. end of EEN (n = 13).*

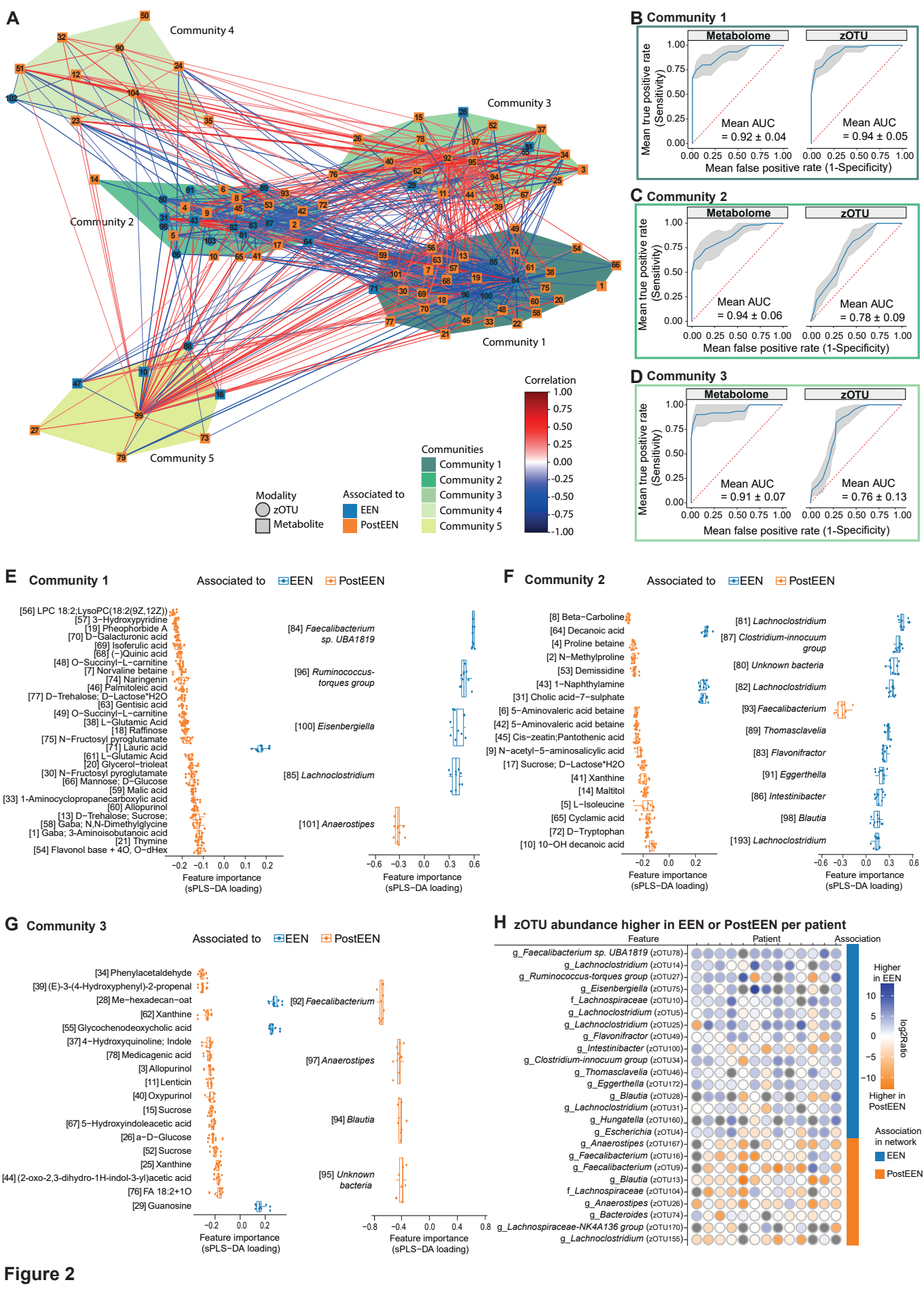
A
Community 1
Community 2
Community 3
Community 4
Community 5
Correlation
1.00
0.75
0.50
0.25
0.00
-0.25
-0.50
-0.75
-1.00
Modality
zOTU
Metabolite
Associated to
EEN
PostEEN
Communities
Community 1
Community 2
Community 3
Community 4
Community 5
B Community 1
Metabolome
zOTU
Mean true positive rate (Sensitivity)
Mean false positive rate (1-Specificity)
Mean AUC = 0.92 ± 0.04
Mean AUC = 0.94 ± 0.05
C Community 2
Mean AUC = 0.94 ± 0.06
Mean AUC = 0.78 ± 0.09
D Community 3
Mean AUC = 0.91 ± 0.07
Mean AUC = 0.76 ± 0.13
E Community 1
Associated to EEN PostEEN
[56] LPC 18:2;LysoPC(18:2(9Z,12Z))
[57] 3−Hydroxypyridine
[19] Pheophorbide A
[70] D−Galacturonic acid
[69] Isoferulic acid
[68] (−)Quinic acid
[48] O−Succinyl−L−carnitine
[7] Norvaline betaine
[74] Naringenin
[46] Palmitoleic acid
[77] D−Trehalose; D−Lactose*H2O
[63] Gentisic acid
[49] O−Succinyl−L−carnitine
[38] L−Glutamic Acid
[18] Raffinose
[75] N−Fructosyl pyroglutamate
[71] Lauric acid
[61] L−Glutamic Acid
[20] Glycerol−trioleat
[30] N−Fructosyl pyroglutamate
[66] Mannose; D−Glucose
[59] Malic acid
[33] 1-Aminocyclopropanecarboxylic acid
[60] Allopurinol
[13] D−Trehalose; Sucrose;
[58] Gaba; N,N-Dimethylglycine
[1] Gaba; 3-Aminoisobutanoic acid
[21] Thymine
[54] Flavonol base + 4O, O−dHex
Feature importance (sPLS−DA loading)
[84] Faecalibacterium sp. UBA1819
[96] Ruminococcus-torques group
[100] Eisenbergiella
[85] Lachnoclostridium
[101] Anaerostipes
F Community 2
[8] Beta−Carboline
[64] Decanoic acid
[4] Proline betaine
[2] N−Methylproline
[53] Demissidine
[43] 1−Naphthylamine
[31] Cholic acid−7−sulphate
[6] 5−Aminovaleric acid betaine
[42] 5−Aminovaleric acid betaine
[45] Cis−zeatin;Pantothenic acid
[9] N−acetyl−5−aminosalicylic acid
[17] Sucrose; D−Lactose*H2O
[41] Xanthine
[14] Maltitol
[5] L−Isoleucine
[65] Cyclamic acid
[72] D−Tryptophan
[10] 10−OH decanoic acid
[81] Lachnoclostridium
[87] Clostridium-innocuum group
[80] Unknown bacteria
[82] Lachnoclostridium
[93] Faecalibacterium
[89] Thomasclavelia
[83] Flavonifractor
[91] Eggerthella
[86] Intestinibacter
[98] Blautia
[193] Lachnoclostridium
G Community 3
[34] Phenylacetaldehyde
[39] (E)-3-(4-Hydroxyphenyl)-2-propenal
[28] Me−hexadecan−oat
[62] Xanthine
[55] Glycochenodeoxycholic acid
[37] 4−Hydroxyquinoline; Indole
[78] Medicagenic acid
[3] Allopurinol
[11] Lenticin
[40] Oxypurinol
[15] Sucrose
[67] 5−Hydroxyindoleacetic acid
[26] a−D−Glucose
[52] Sucrose
[25] Xanthine
[44] (2-oxo-2,3-dihydro-1H-indol-3-yl)acetic acid
[76] FA 18:2+1O
[29] Guanosine
[92] Faecalibacterium
[97] Anaerostipes
[94] Blautia
[95] Unknown bacteria
H zOTU abundance higher in EEN or PostEEN per patient
Feature
Patient
Association
g_Faecalibacterium sp. UBA1819 (zOTU78)
g_Lachnoclostridium (zOTU14)
g_Ruminococcus-torques group (zOTU27)
g_Eisenbergiella (zOTU75)
f_Lachnospiraceae (zOTU10)
g_Lachnoclostridium (zOTU5)
g_Lachnoclostridium (zOTU25)
g_Flavonifractor (zOTU49)
g_Intestinibacter (zOTU100)
g_Clostridium-innocuum group (zOTU34)
g_Thomasclavelia (zOTU46)
g_Eggerthella (zOTU172)
g_Blautia (zOTU28)
g_Lachnoclostridium (zOTU31)
g_Hungatella (zOTU160)
g_Escherichia (zOTU4)
g_Anaerostipes (zOTU167)
g_Faecalibacterium (zOTU16)
g_Faecalibacterium (zOTU9)
g_Blautia (zOTU13)
f_Lachnospiraceae (zOTU104)
g_Anaerostipes (zOTU26)
g_Bacteroides (zOTU74)
g_Lachnospiraceae-NK4A136 group (zOTU170)
g_Lachnoclostridium (zOTU155)
Higher in EEN
log2Ratio
Higher in PostEEN
Association in network
EEN
PostEEN

Figure 2

***Fig. 2: Data integration and identification of features for EEN**:*

***A** Correlation network built from selected features based on sPLS-DA-based data integration. Five communities were identified (color coded as indicated). Indicated are zOTUs (circles) and metabolites (squares), their associations to EEN (blue) or PostEEN (orange), and correlation values (lines between features, blue to red). **B - D** ROC curves for metabolome and zOTU features, respectively, for Community 1, 2, and 3. **E - G** Most important features (i.e., metabolites and zOTUs) for each community with their feature importance for PostEEN (<0, orange) and EEN (>0, blue). One dot represents the loading of the respective feature for a single iteration of the cross-validation procedure (i.e. each iteration is trained on a (stratified) random subset of all data points). **H** Dotplot of patient-specific expression levels of EEN and PostEEN zOTU signatures (N = 13; all of which EEN and PostEEN samples were available) showing individual log fold-changes between expression levels of EEN and PostEEN samples. The mean of expression was used when more than one sample was available per patient and condition, i.e. EEN or PostEEN. Blue, higher expression in EEN samples; orange, higher expression levels in PostEEN samples; white, balanced between conditions; grey, zOTU was not present in the EEN and PostEEN sample.*

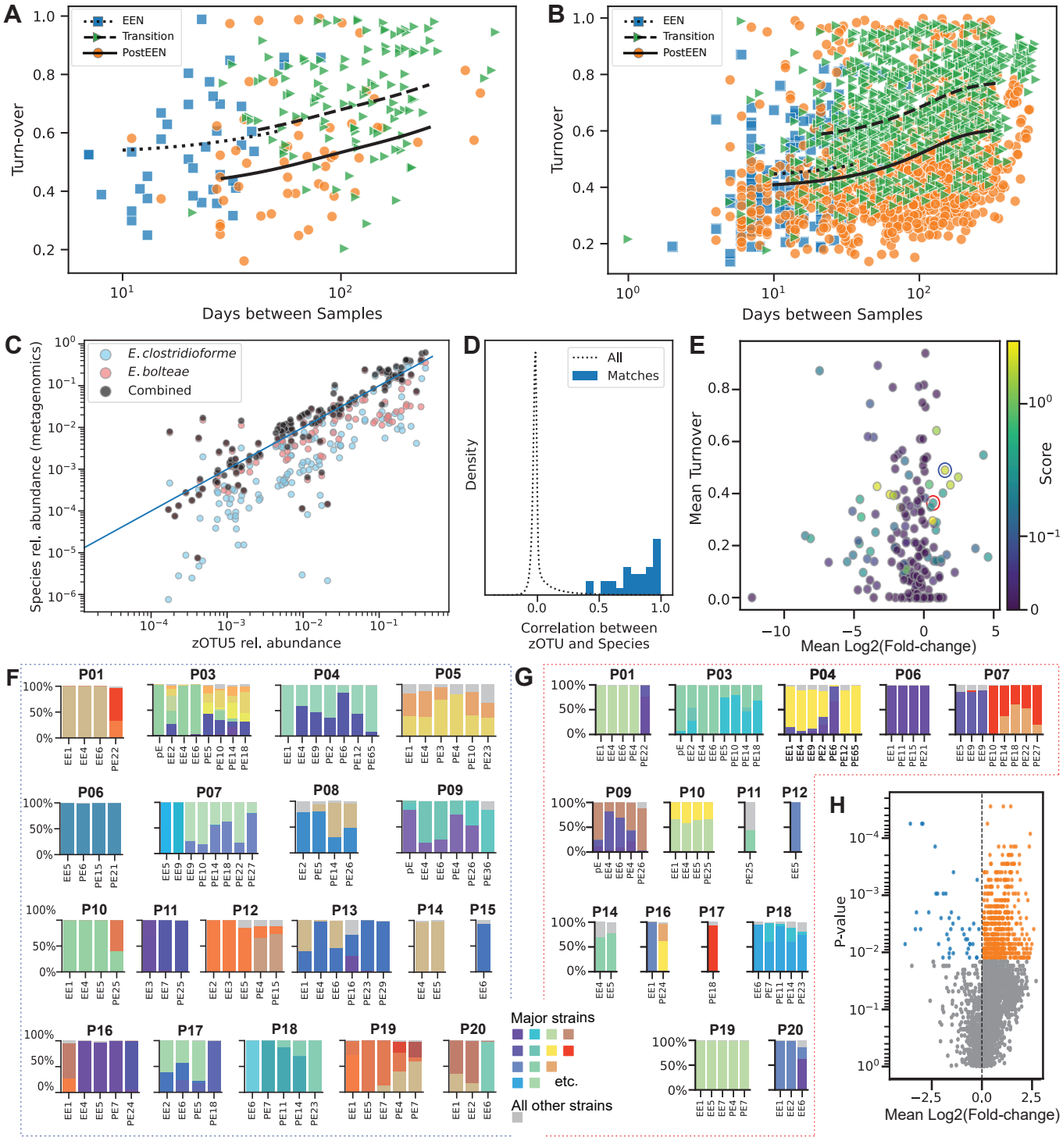
A
EEN
Transition
PostEEN
Turn-over
Days between Samples
B
Turnover
C
E. clostridioforme
E. bolteae
Combined
Species rel. abundance (metagenomics)
zOTU5 rel. abundance
D
All
Matches
Density
Correlation between zOTU and Species
E
Mean Turnover
Mean Log2(Fold-change)
Score
F
G
Major strains
etc.
All other strains
H
P-value
Mean Log2(Fold-change)

Figure 3

Fig. 3 – Species and strain turnover during the transition off of EEN:

A, B *Turnover of taxonomic composition during the transition from EEN to a PostEEN diet of both* ***(A)*** *strain and* ***(B)*** *zOTU compositions. The three lines reflect cubic spline regression of Bray-Curtis dissimilarities against time, averaged across subjects and offset by an independent intercept for each pair type.* ***C*** *Correlation between the relative abundance of zOTU5 and the individual and combined relative abundances of the species* Enterocloster bolteae *and* Enterocloster clostridioforme *determined by quantification with shotgun metagenomes. The blue diagonal represents a 1:1 relationship in relative abundance.* ***D*** *The distribution of correlations between zOTUs and species. The 27 pairs matched in this way (****Extended Data Table 1****), including zOTU5 with each of* E. bolteae *and* E. clostridioforme*, had substantially greater Pearson correlation than unmatched pairs ($p<10^{-10}$, Mann-Whitney U test).* ***E*** *Characterization of species based on fold-change in relative abundance between EEN and PostEEN samples and average strain-level turnover, defined as the mean Bray-Curtis dissimilarity between within-subject sample pairs. Particularly interesting species were identified based on the product of these two statistics, the number of within-subject sample pairs, and the mean relative abundance (****Extended Data Table 1****). Points are colored based on this score, and the two species matched to zOTU5 are circled:* E. bolteae *(blue),* E. clostridioforme *(red). Plots for the 20 highest scoring species are in* ***Supplementary Fig. 2. F, G*** *Composition over time of strains within* ***(F)*** E. bolteae *(blue box) and* ***(G)*** E. clostridioforme *(red box),* both abundant in the CD-EEN patients: Both species have *noteable strain dynamics during and after EEN, but with* E. bolteae *showing higher diversity and turnover. Strain genotypes and fractions were estimated from shotgun metagenomic data. Fractions of abundant strains (colored bars) are shown across samples from individual subjects (P01, P02…), before EEN ("pE" labels on x-axis), during ("EE") and after ("PE"). Strain fractions for the species sum to 1.0; minor strains are summed together and shown in grey.* ***H*** *Volcano plots showing COG functions with significant changes in normalized abundance at the transition off of EEN (red; Wilcoxon test at false discovery rate (FDR) < 0.1). 45 COGs were at significantly greater relative depth during PostEEN and 532 during EEN.*

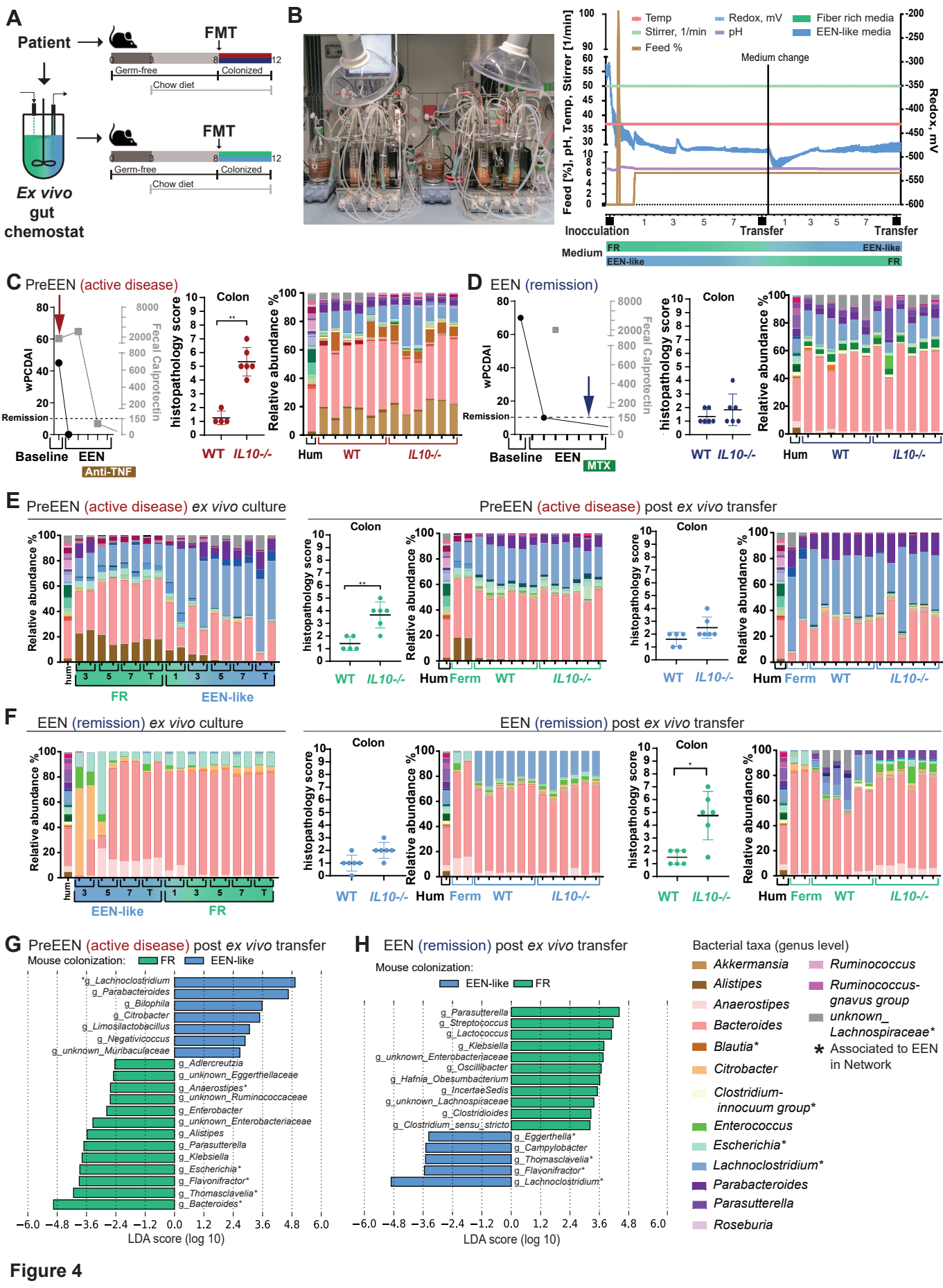
A
Patient
FMT
Germ-free
Colonized
Chow diet
Ex vivo gut chemostat
B
Temp
Stirrer, 1/min
Feed %
Redox, mV
pH
Fiber rich media
EEN-like media
Medium change
Feed [%], pH, Temp, Stirrer [1/min]
Redox, mV
Inocculation
Transfer
Medium
FR
EEN-like
C PreEEN (active disease)
wPCDAI
Fecal Calprotectin
Remission
Baseline
EEN
Anti-TNF
Colon
histopathology score
Relative abundance %
WT
IL10-/-
Hum
D EEN (remission)
MTX
E PreEEN (active disease) ex vivo culture
PreEEN (active disease) post ex vivo transfer
Ferm
F EEN (remission) ex vivo culture
EEN (remission) post ex vivo transfer
G PreEEN (active disease) post ex vivo transfer
Mouse colonization: FR EEN-like
g_Lachnoclostridium
g_Parabacteroides
g_Bilophila
g_Citrobacter
g_Limosilactobacillus
g_Negativicoccus
g_unknown_Muribaculaceae
g_Adlercreutzia
g_unknown_Eggerthellaceae
g_Anaerostipes*
g_unknown_Ruminococcaceae
g_Enterobacter
g_unknown_Enterobacteriaceae
g_Alistipes
g_Parasutterella
g_Klebsiella
g_Escherichia*
g_Flavonifractor*
g_Thomasclavelia*
g_Bacteroides*
LDA score (log 10)
H EEN (remission) post ex vivo transfer
Mouse colonization: EEN-like FR
g_Parasutterella
g_Streptococcus
g_Lactococcus
g_Klebsiella
g_unknown_Enterobacteriaceae
g_Oscillibacter
g_Hafnia_Obesumbacterium
g_IncertaeSedis
g_unknown_Lachnospiraceae
g_Clostridioides
g_Clostridium_sensu_stricto
g_Eggerthella*
g_Campylobacter
g_Thomasclavelia*
g_Flavonifractor*
g_Lachnoclostridium*
Bacterial taxa (genus level)
Akkermansia
Alistipes
Anaerostipes
Bacteroides
Blautia*
Citrobacter
Clostridium-innocuum group*
Enterococcus
Escherichia*
Lachnoclostridium*
Parabacteroides
Parasutterella
Roseburia
Ruminococcus
Ruminococcus-gnavus group
unknown_Lachnospiraceae*
* Associated to EEN in Network

Figure 4

Fig. 4: Functional validation of gut microbiota-dependent EEN-efficacy using* ex vivo *fermentation and gnotobiotic humanized mice.

A *Experimental scheme: Patient sample is transferred into GF mice at the age of 8 weeks for 4 weeks. Same patient sample is also transferred in an* ex vivo *gut chemostat model and treated with medium simulating EEN (EEN-like, devoid of fibers) or a regular diet (fiber-rich, FR). Fermented sample is transferred (post* ex vivo*) into GF mice (age of 8 weeks) for 4 weeks.* ***B*** *Assembly of the* ex vivo *gut chemostat model. Samples are fermented in technical duplicates. Parameters are recorded over the full course of the experiment and plotted as seen: feed, pH, temperature, stir speed and redox potential. Depending on the sample's origin, the start medium is chosen to match the diet of the patient at time of sample collection (PreEEN on FR media, EEN on EEN-like media) with a switch to the respective other medium in between.* ***C, D*** *Transfer of patient sample: patients disease state with wPCDAI and fecal calprotectin levels, therapy response over time with maintenance therapy (MTX, Anti-TNF) and sampling time point, histopathology scoring of colon Swiss roles of recipient mice after 4 weeks of colonization, 16S rRNA gene sequencing of colonic content after 4 weeks of colonization. H&E in supplement Fig. 5.* ***C*** *PreEEN (active) sample transfer.* ***D*** *EEN (remission) sample transfer.* ***E,F*** Ex vivo *continuous culture of human fecal sample using different media performed in one experiment with transfer (timepoint, T) into a mouse model at the end of each medium exposure. Shown are the histopathology scoring of colon Swiss roles and 16S rRNA gene sequencing analyses, together with initial donor sample, fermented transfer sample and recipient mice colonic content after 4 weeks of colonization. H&E in Extended Data Fig. 3.* ***E*** Ex vivo *fermentation of PreEEN (active) sample, start under FR medium and switch to EEN-like medium followed by mouse data from the FMT after 4 weeks of colonization (green: FR conditioned post* ex vivo *microbiota transfer; blue: EEN conditioned post* ex vivo *microbiota transfer).* ***F*** Ex vivo *fermentation with EEN (remission) sample, start under EEN-like medium and switch to FR media.* ***G*** *LEfSe (Linear discriminant analysis Effect Size) analysis of differentially abundant bacteria at genus level in the post* ex vivo *recipient mice of fermented PreEEN fecal sample (mouse colonization: FR = mice received PreEEN sample fermented under FR media; EEN-like = mice received PreEEN sample fermented under consecutive EEN-like media).* ***H*** *LEfSe analysis of differentially abundant bacteria at genus level in the post* ex vivo *recipient mice of fermented EEN fecal sample (mouse colonization: EEN-like = mice received EEN sample fermented under EEN-like media; mouse FR = mice received EEN sample fermented under consecutive FR media). 16S rRNA gene sequencing analyses is color coded for the 16 most abundant taxa at genus level. * indicates genera identified in data integration network analyses associated to EEN (based on zOTUs), respectively. Hum = human donor sample; Ferm = Fermenter Transfer (T) sample. Data are represented by (**C, D, E, F**) mean ± SD of six biological replicates. P values were calculated by Mann-Whitney test. *P<0.05, **P<0.01, ***P<0.001, ****P<0.0001.*

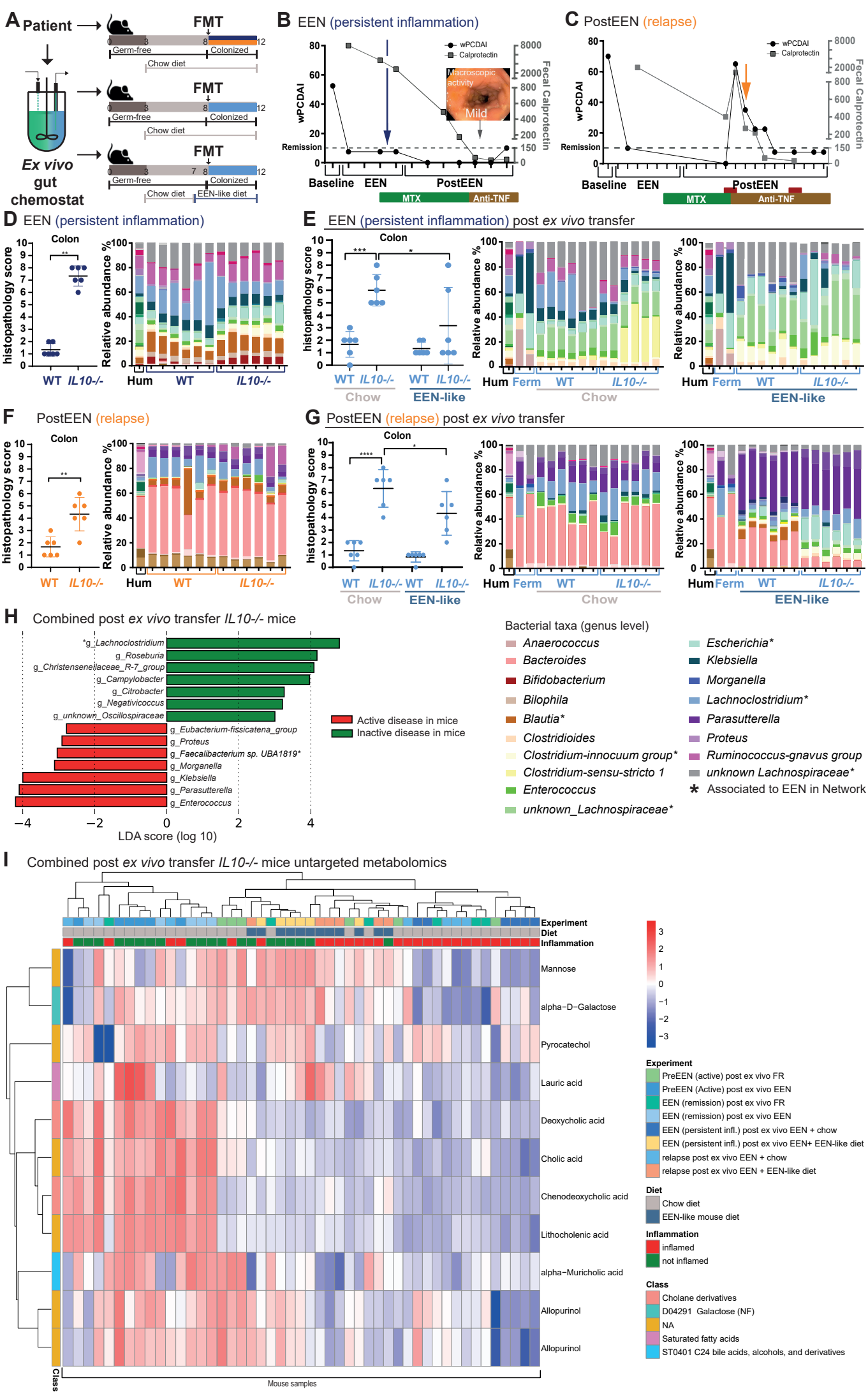
A Patient
Ex vivo gut chemostat
FMT
Germ-free
Colonized
Chow diet
EEN-like diet
B EEN (persistent inflammation)
wPCDAI
Calprotectin
Fecal Calprotectin
Macroscopic activity
Mild
Remission
Baseline
EEN
PostEEN
MTX
Anti-TNF
C PostEEN (relapse)
D EEN (persistent inflammation)
Colon
histopathology score
Relative abundance %
WT
IL10-/-
Hum
E EEN (persistent inflammation) post ex vivo transfer
Ferm
Chow
EEN-like
F PostEEN (relapse)
G PostEEN (relapse) post ex vivo transfer
H Combined post ex vivo transfer IL10-/- mice
*g_Lachnoclostridium
g_Roseburia
g_Christensenellaceae_R-7_group
g_Campylobacter
g_Citrobacter
g_Negativicoccus
g_unknown_Oscillospiraceae
g_Eubacterium-fissicatena_group
g_Proteus
g_Faecalibacterium sp. UBA1819*
g_Morganella
g_Klebsiella
g_Parasutterella
g_Enterococcus
Active disease in mice
Inactive disease in mice
LDA score (log 10)
Bacterial taxa (genus level)
Anaerococcus
Bacteroides
Bifidobacterium
Bilophila
Blautia*
Clostridioides
Clostridium-innocuum group*
Clostridium-sensu-stricto 1
Enterococcus
unknown_Lachnospiraceae*
Escherichia*
Klebsiella
Morganella
Lachnoclostridium*
Parasutterella
Proteus
Ruminococcus-gnavus group
unknown Lachnospiraceae*
* Associated to EEN in Network
I Combined post ex vivo transfer IL10-/- mice untargeted metabolomics
Experiment
Diet
Inflammation
Mannose
alpha−D−Galactose
Pyrocatechol
Lauric acid
Deoxycholic acid
Cholic acid
Chenodeoxycholic acid
Lithocholenic acid
alpha−Muricholic acid
Allopurinol
Allopurinol
Class
Mouse samples
PreEEN (active) post ex vivo FR
PreEEN (Active) post ex vivo EEN
EEN (remission) post ex vivo FR
EEN (remission) post ex vivo EEN
EEN (persistent infl.) post ex vivo EEN + chow
EEN (persistent infl.) post ex vivo EEN+ EEN-like diet
relapse post ex vivo EEN + chow
relapse post ex vivo EEN + EEN-like diet
Chow diet
EEN-like mouse diet
inflamed
not inflamed
Cholane derivatives
D04291 Galactose (NF)
NA
Saturated fatty acids
ST0401 C24 bile acids, alcohols, and derivatives

Figure 5

***Fig. 5: Low-fiber diet lowered inflammation in humanized gnotobiotic mice**:*

***A** Experimental scheme: Patient sample is transferred into GF mice at the age of 8 weeks, for 4 weeks. Same patient sample is also transferred in an* ex vivo *gut chemostat model and treated with different media. Fermented sample is transplanted (post* ex vivo*) into GF mice at the age of 8 weeks, for 4 weeks getting either chow diet or EEN-like purified diet (EEN-like) one week prior to FMT. **B** Selected patient sample for transfer (persistent inflammation): patients' disease state with wPCDAI and fecal calprotectin, therapy response over time, maintenance therapy (MTX, Anti-TNF) and sampling time point of transferred fecal sample (blue arrow); grey arrow indicates endoscopy performed in the patient PostEEN and the picture taken during endoscopy shows active ileitis. **C** Selected patient sample for transfer (relapse): patients' disease state with wPCDAI and fecal calprotectin, therapy response over time, maintenance therapy (MTX, Anti-TNF) and sampling time point of transferred fecal sample (orange arrow). **D** Histopathology scoring of colon Swiss roles of recipient mice from the direct transfer of EEN (persistent inflammation) sample and 16S rRNA gene sequencing of colonic content after 4 weeks of colonization. H&E in Extended Data Fig. 3. **E** EEN (persistent inflammation) post* ex vivo *FMT results: Histopathology score of colon Swiss roles after 4 weeks of colonization from subsequent FMT after* ex vivo *fermentation under EEN-like medium (grey bar below: EEN-conditioned microbiota transfer on chow; dark blue bar below: EEN-conditioned microbiota transfer on EEN-like mouse diet) with 16S rRNA gene sequencing of colonic content in the recipient mice under chow diet (grey) or EEN-like diet (dark blue). H&E in Extended Data Fig. 3. **F** Histopathology scoring of colon Swiss roles of recipient mice from the direct transfer of PostEEN relapse sample and 16S rRNA gene sequencing of colonic content after 4 weeks of colonization. H&E in Extended Data Fig. 3. **G** PostEEN (relapse) post* ex vivo *FMT results: Histopathology score of colon Swiss roles after 4 weeks of colonization from subsequent FMT after* ex vivo *fermentation under EEN like medium (grey bar below: EEN-conditioned microbiota transfer on chow; dark blue bar below: EEN-conditioned microbiota transfer on EEN-like mouse diet) with 16S rRNA gene sequencing of colonic content in the recipient mice under chow diet (grey) or EEN-like diet (dark blue). H&E in Extended Data Fig. 3. **H** Combined LEfSe analysis of differentially abundant bacteria at genus level in inflamed vs. non-inflamed IL10$^{-/-}$ post* ex vivo *transfer. A histopathology score >3 was considered as inflamed phenotype. **I** Differential heat map (based on Wilcoxon test) of untargeted metabolomics measured in IL10$^{-/-}$ mice from post* ex vivo *experiments. Samples clustered according to inflammation and their similarity of metabolite features. Color codes on top indicate the experiment, diet (chow, EEN-like), and classification of inflammation ('inflamed' if histopathology score >3). Color code on the left indicates metabolite classes. * indicates genera identified in data integration network analyses associated to EEN (based on zOTUs). Hum = human donor sample; Ferm = Fermenter Transfer (T) sample. Data are represented by (**D, E, F, G**) mean ± SD of six biological replicates. P values were calculated by Mann-Whitney test or ANOVA followed by pairwise comparison testing (Tukey). *P<0.05, **P<0.01, ***P<0.001, ****P<0.0001.*

Material and Methods

Patient cohort, recruitment and study design

Patients (aged 3-18 years) with suspected or established IBD were recruited to a monocentric pediatric IBD cohort study (ethics approval Ludwig-Maximilians University of Munich, approval No. 17-801 and German Clinical Trials Register accession No. DRKS00013306, date registration 19.03.2018). All patients and parents/legal guardians provided written informed consent/assent. Patients without confirmed IBD after full diagnostic work-up according to revised Porto criteria were excluded[37]. All other patients were followed prospectively for one year and treated according to current ESPGHAN/ECCO guidelines for CD or ulcerative colitis (UC)/IBD unclassified (IBDU) [6,38,39]. Disease activity, as well as endoscopic, histologic, radiologic and laboratory findings were collected prospectively. Disease activity indices included the Physician Global Assessment (PGA) and the weighted pediatric Crohn's disease activity index (wPCDAI) for CD, as well as the pediatric ulcerative colitis activity index (PUCAI) for UC/IBDU. For EEN-treated CD patients, remission was defined as wPCDAI <12.5 points and response as reduction in wPCDAI of >17.5 points, but not reaching remission. Relapse was defined as increase of wPCDAI ≥12.5 points and/or fecal calprotectin >250 mg/L requiring changes in medical treatment or abdominal surgery or reintroduction of EEN. Patients received detailed instructions for fecal specimen collections and time points, as well as stool collection kits. Each sample was accompanied with a questionnaire on date and time of specimen collection, problems during sampling, Bristol Stool Scale and recent antibiotic use.

EEN therapy was prescribed for 6-8 weeks, followed by gradual re-introduction of solid food and concomitant start of maintenance treatment. EEN was performed with Modulen® IBD (Nestlé Health Science) or in case of intolerance (e.g. cow's milk protein allergy) with Neocate Junior® (Nutricia, Erlangen, Germany). The amount of prescribed formula was based on the Daily Recommendations Intake (DRI) using the online calculator: https://www.nal.usda.gov/human-nutrition-and-food-safety/dri-calculator. EEN-treated patients received dietary advice.

Fecal specimen collection

Samples were collected at home or in the hospital. Patients provided samples at baseline (before bowel preparation for endoscopy) and every four weeks in (1) 4 mL DNA stabilizer (magiX PBI Microbiome Preservation Buffer, microBIOMix GmbH, Regensburg)[40], (2) 8 mL 20% glycerol in reduced phosphate-buffered saline (PBS, 0.05% L-cysteine) and (3) naïve without stabilizing solution. Patients on EEN collected stool in (1) weekly for the first 12 weeks. Samples in (1) were shipped at ambient temperature by mail to the study center. Fecal specimens in (2) and (3) were immediately frozen at home (approx. -18 to -20°C) and brought

in on wet ice packs at the next visit. Upon receipt, samples were aliquoted, barcoded, linked to clinical data with CentraXX Bio (Kairos GmbH) and stored immediately at -80°C until further analysis.

Selection of donor samples for transfer experiments into germ-free mice

Stool samples for FMT experiments into germ-free (GF) mice were selected according to the following criteria: active disease included samples from treatment-naive patients before the start of EEN (PreEEN), EEN-induced remission (EEN) or reintroduction of a regular diet (PostEEN).

Animal ethics statement

All animal experiments were conducted at Technical University of Munich and approved by the Committee on Animal Health Care and Use of the State of Upper Bavaria (TVA ROB-55.2-2532.Vet_02-19-190) and performed in strict compliance with the EEC recommendations for the care and use of laboratory animals (European Communities Council Directive of November 24, 1986 (86/609/EEC).

Animals and housing conditions

GF wild-type (WT) and IL-10-deficient (*IL10*$^{-/-}$) mice on 129Sv/Ev background were kept at the Gnotobiology Core Facility of the ZIEL Institute for Food & Health, Technical University of Munich, Freising, Germany. Mice were housed as described elsewhere[17], but using single gnoto-cage units (Isocage P System, Tecniplast, Italy). Cages are ventilated with HEPA-filtered air at 22 ± 1°C with a 12-h light/dark cycle. Female and male mice were assigned randomly to the treatment groups with a ratio of 1:1 and six mice per genotype. Mice received standard chow (V1124-300; Ssniff, Soest, Germany; autoclaved) or an EEN-like purified diet (EEN-like, SNIFF S5745-E902, Supplement Fig. 1D) and sterile water *ad libitum*. EEN-like diet was introduced one week prior to fecal microbial transfer (FMT) to allow for adaptation. Handling of mice in isocages was performed under biological safety cabinets in sterile conditions.

Preparing gavage for humanizing germ-free mice

Preparation of FMT with human fecal microbiota was performed according to Metwaly *et al*. (2020)[17]. For post *ex vivo* FMT, frozen samples in glycerol (20% end concentration) were thawed on ice. All steps were performed in an anaerobic chamber (90% N_2 and 10% H_2). *Ex vivo* suspensions (2 mL) were centrifuged at 100×*g* for 3 min at 4°C to pellet debris. Supernatant was collected and centrifuged at 8000×*g* for 10 min at 4°C to pellet the bacteria. The bacterial pellet was resuspended in 1.5 mL reduced PBS (0.05% L-cysteine-HCl). The clear supernatant was transferred into an anaerobic crimped tube, which was transferred to

the gnotobiotic facility. All mice were gavaged on three consecutive days and sacrificed after four weeks of colonization (12 weeks of age).

Tissue Staining and scoring

Colonic and cecal Swiss-roll tissues were fixed, stained and scored as described before[17]. In brief, tissue was fixed in 4% formaldehyde/PBS for 48 h at room temperature, subsequently dehydrated (Leica TP1020), and embedded in paraffin (McCormick; Leica EG1150C). Formalin-fixed paraffin-embedded (FFPE) tissue sections were stained with hematoxylin and eosin (H&E) and scored 0 (not inflamed) to 12 (highly inflamed).

***Ex vivo* gut chemostat model**

The *ex vivo* continuous fermentation was performed in 1.4-L bioreactors (Multifors 2) and monitored with Eve®software (Infors AG, Basel, Switzerland). Parameters were set as described before[41]. Briefly, vessels were maintained at 37°C, pH 6.8 with a constant influx of N_2 to maintain an anaerobic atmosphere. Inoculation material was prepared in an anaerobic chamber (90% N_2 and 10% H_2). Approximately 2.5 g of frozen fecal samples was suspended in reduced PBS supplemented with 0.03 g/mL L-cysteine-HCl, filtered (70 µm Cell Strainer, FisherScientific) and evenly distributed between two vessels, which led to about 1.0×10^8 to 8.16×10^8 CFU/vessel. Two consecutive batch fermentations (24 h in 400 mL, another 24 h with fresh 400 mL medium added) allowed fecal microbial communities to establish. Continuous fermentation included complete medium exchange every 36 h (retention time) with a working volume of 400 mL. After 10 days of continuous fermentation, where stable community formation was achieved, samples for transfer into GF mice were collected and medium was switched afterwards. After 1.5 days of complete medium exchange from medium 1 to medium 2, samples for transfer into mice were collected on day 9 of continuous fermentation in the second medium. Medium composition was either fiber-rich (FR) or EEN-like, mimicking patient conditions at sampling (PreEEN and PostEEN, respectively; Supplement Fig. XC).

FR medium was prepared according to Macfarlane *et al*. (1998)[42], but supplemented with additional vitamins (pantothenate 10 mg/L, nicotinamide 5 mg/L, thiamine 4 mg/L, biotin 2 mg/L, vitamin B12 0.5 mg/L, menadione, 1 mg/L and p-aminobenzoic acid 5 mg/L) as described in Gibson and Wang[43]. EEN-like medium was based on the Macfarlane medium, but with modifications simulating colonic-luminal content during an EEN diet. To determine the carbohydrate:protein ratio of digested Modulen IBD® in the colon, similar calculations as described previously were conducted[44,45]. Since Modulen IBD® lacks fibers, these ingredients present in the FR medium (i.e., pectin from citrus, guar gum, xylan from oat spelt, inulin from *Dahlia* tubers, and arabinogalactan from larch wood) were replaced by soluble rice starch and simple sugars. A total carbohydrate concentration of 13 g/L was chosen in alignment with

Cinquin *et al.* (2004)[44]. As the formulation of Modulen IBD® is not publicly available, we decided to include some Modulen IBD® not to miss crucial nutrients in our model-colon medium. Towards this end, 10% v/w of Modulen IBD® was added to the EEN-like medium. Finally, the carbohydrate:protein ratio was 75:25 in the model medium. To further mimic Modulen IBD®, casein was used as main protein source with the exclusion of tryptone and peptone (Supplement Fig. 1A-C).

Samples were aseptically collected daily at the same daytime and stored at -80°C until further analyses. Samples for transfer into the GF mice were collected and mixed with glycerol (20% end concentration) and stored at -80°C until gavage preparation. In order to diminish potential vessel effects in the technical duplicates of each fermenter colonization, samples from both vessels were mixed 50:50 for gavage.

High-throughput 16S-ribosomal RNA (rRNA) gene amplicon sequencing analysis

Total DNA from human stool, colonic mouse content and the continuous *ex vivo* fermentation was isolated using bead beating and sequenced for 16S-rRNA gene amplicons as described[46]. Downstream analysis was performed in R v4.2.1 using Rhea (https://lagkouvardos.github.io/Rhea/)[47]. zOTU tables were normalized to 10.000 reads, beta-diversity was computed using generalized UniFrac distances[48]. Alpha-diversity was assessed on the basis of taxa richness and Shannon effective number of zOTUs[49]. Trees were visualized and annotated using EvolView (http://www.evolgenius.info/evolview/)[50]. Differential analyses of bacteria in different groups was done using LDA Effect Size (LEfSe)[51].

Shotgun Metagenomic Sequencing and Analysis

Metagenomic sequencing was performed for 96 human stool samples and 66 samples from transfer experiments (54 mouse, 12 ex vivo) using the genomic DNA already isolated for 16S-rRNA gene amplicon sequencing. DNA was randomly sheared into short fragments. The obtained fragments were end repaired, A-tailed, and further ligated with Illumina adapters. The fragments with adapters were size-selected, PCR amplified, and purified. The library was checked with Qubit and real-time PCR for quantification and BioAnalyzer for size distribution detection as required by Illumina (TruSeq® DNA Library Prep Kit). Quantified libraries were pooled and sequenced on a NovaSeq platform (Illumina) in PE150 mode. Raw data were aimed at 15 Gb per demultiplexed sample. From raw shotgun metagenomic sequencing data, adapter sequences were removed using Trimmomatic v0.39 [52] without considering any mismatch and parameters LEADING:3, TRAILING:3, and SLIDINGWINDOW:4:15. We removed human reads by mapping against human reference genome hg38 by using Bowtie2 v2.4.5 [53] with the default parameters. Cleaned fastq data files were used in the following steps.

Strain tracking and strain gene content analyses were performed based on the StrainPGC workflow [@Smith2023, https://github.com/bsmith89/StrainPGC]. Briefly, preprocessed metagenomes were metagenotyped using GT-Pro v1.0.1[54]. Across all samples, 369 species - as defined in the Unified Human Gut Genome (UHGG)[55]—were robustly detected and only these were included in downstream pangenome profiling. Single nucleotide polymorphism (SNP) profiles were filtered, subsampled, and strain relative abundances were estimated with StrainFacts v0.4.0[16]. Within individual species, estimated strain fractions add up to 100%. By contrast, other analyses considered the overall strain composition: the relative abundance of each strain across all species.

Gene profiling was performed against a subset of the MIDASDB-UHGG pangenome database[56] v1.5 dereplicated at a 99% ANI threshold performed and mapping reads using Bowtie2 v2.4.5 [53]. Species abundances were estimated based on the average depth of core genes. Global functional gene family profiling was performed by aggregating gene depths into Clusters of Orthologous Genes (COGs) across all species and then normalizing based on 25 ubiquitous, single-copy genes to estimate “gene copies per genome”.

Metabolomics

Approximately 20 mg of mouse colon content was weighed in a 2-mL bead-beating tube (Matrix D, MP Biomedicals Germany GmbH, Eschwege, Germany) and was extracted with 1 mL of methanol-based dehydrocholic acid extraction solvent (c = 1.3 µmol/L) according to *Reiter et al*.[57]. For the fermenter samples and human fecal samples, 200 mg and 100 mg, respectively, were weighed in a 15-mL bead-beating tube (Matrix D) and extracted with 5 mL extraction solvent as above. The untargeted data was generated and processed according to Weiss *et al*[58].

Data integration of 16s rRNA amplicon data with metabolomics and metagenomics

We matched 60 samples from 15 patients of the 16S-rRNA gene sequencing to 60 samples of the untargeted metabolomics analysis according to patient ID and same time points. The aim was to discriminate features between 23 EEN samples (clinical phenotype mild and remission) and 37 PostEEN samples (>2 weeks after EEN, clinical remission). For the integrated selection of metabolome and microbiota features, sparse Partial Least Squares-Discriminant Analysis (sPLS-DA) function from the DIABLO framework (mixOmics version 6.20) was used[59]. For feature selection concerning metabolomics, only annotated metabolites were considered. Input metabolites were mean centered and scaled to unit variance, while zOTUs were centered log-ratio transformed. To estimate the degree of overfitting, the model was trained on 70% of the data, with a k-fold cross-validation for feature selection during training. The remaining 30% of the data were used to evaluate the generalization power. The model performance was measured with an Area Under the Receiver Operating Characteristic (ROC-AUC). This

procedure was done once with the actual labels and 200-times with randomized labels, to obtain an empirical p-value for the model prediction on the validation data. Subsequently, Spearman's rank correlation coefficients between all selected metabolites and zOTUs were computed and their respective p-values were corrected with the Benjamini-Hochberg procedure[60]. All coefficients with an FDR >0.05 were set to 0. Using all non-zero correlations, a network was generated and the Louvain method for community detection[61] was applied to extract highly connected subgraphs from the correlation network. For each community, a PLS-DA model was trained with the same train-test and randomization scheme explained previously for feature selection. Feature importance was plotted using the loadings in each iteration and determining their association to either EEN or PostEEN. Analyses were run in R v4.2.1 and python v3.8.11. For network analysis the igraph v1.3.4[62] and networkx v3.1[63] packages were used.

Profiles of 16S rRNA amplicon relative abundance were further integrated with metagenomic species profiles in order to identify those which represent the same, underlying taxa. This was done by calculating the Pearson correlation coefficient between each zOTU relative abundance and species relative abundances estimated from the metagenomic workflow. Each correlation was then weighted by the mean relative abundance of that zOTU and species, respectively, producing a matrix of matching scores for each comparison. Based on this score, we ranked zOTUs for each species and species for each zOTU. We selected as putative matches all zOTU-species pairs that were either reciprocal best hits or a combination of one best hit and one second-best hit. In this way, we accounted for the possibility of multiple zOTUs representing a species or multiple species being represented by a zOTU.

Statistical analysis

Significances of metabolic features from the post *ex vivo* fermentation experiment were computed with Wilcoxon signed-rank tests and FDR-corrected using the Benjamin-Hochberg method. Subsequent hierarchical clustering using only differentially abundant metabolites ($q < 0.05$) was conducted using complete linkage based on Euclidean distances. Calculations, as well as heatmaps, were computed in R v4.2.1. Further statistical analyses and plots were generated using GraphPad Prism v8.0 (GraphPad, La Jolla, CA) using Mann-Whitney test, analysis of variance (ANOVA) followed by pairwise comparison testing (Tukey, Bonferroni correction), by Kruskal-Wallis test followed by Dunn`s multiple comparisons. Data is presented as mean ± SD. P-values below 0.05 were considered significant ($p<0.05$, *; $p<0.01$, **; $p<0.001$, ***; $p<0.0001$, ****).

Taxonomic turnover in both zOTU and strain compositions were calculated based on the Bray-Curtis dissimilarity. Pairs where one sample was collected during EEN and the other during

PostEEN were classified as “transition”. All within-subject pairwise comparisons were computed and fit using cubic spline regression of the time between sample collections, with a regression term for each subject, as well as for each pair class: EEN, transition, or PostEEN. The null hypothesis of no difference between pair classes was tested by permutation: 999 random permutations of samples within subjects. Changes in mean, normalized, COG depths during EEN and PostEEN time points were tested using the Wilcoxon signed-rank test across subjects. False discovery rates were calculated using the Benjamini-Hochberg procedure. Mean fold change for each COG was calculated as the ratio between these two estimates.

Data availability

The data that support the findings of this study are available on reasonable request from the corresponding author [TS]. The data are not publicly available due to the pediatric age of the research participants.

Code availability

Mutliomic data integration of 16S rRNA and metabolomics code is available at https://github.com/nklkhlr/een-multiomics. All code necessary to reproduce the metagenomic data analysis will be made publicly available on GitHub at the time of publication, or is available upon request.